buildings

MDPI

Article

Petrological Characteristics and Physico-Mechanical Properties of Dokhan Volcanics for Decorative Stones and Building Material Applications

El Saeed R. Lasheen [1,*], Mabrouk Sami [2,3,*], Ahmed A. Hegazy [4], Hasan Arman [2], Ioan V. Sanislav [5], Mohamed S. Ahmed [6] and Mohammed A. Rashwan [7,*]

1 Geology Department, Faculty of Science, Al-Azhar University, Cairo 11884, Egypt
2 Geosciences Department, College of Science, United Arab Emirates University, Al Ain 15551, United Arab Emirates
3 Department of Geology, Faculty of Science, Minia University, El-Minia 61519, Egypt
4 Refractories, Ceramics, and Building Materials Department, National Research Centre, 33 El Bohooth St. (Former El Tahrir St.)—Dokki, Giza P.O. Box 12622, Egypt
5 College of Science and Engineering, James Cook University, Economic Geology, Townsville, QLD 4811, Australia
6 Geology and Geophysics Department, College of Science, King Saud University, P.O. Box 2455, Riyadh 11451, Saudi Arabia
7 Geological Sciences Department, National Research Centre, 33 El Bohooth St. (Former El Tahrir St.)—Dokki, Giza P.O. Box 12622, Egypt
* Correspondence: elsaeedlasheen@azhar.edu.eg (E.S.R.L.); mabrouksami@uaeu.ac.ae (M.S.); ma.attia@nrc.sci.eg (M.A.R.)

Abstract: Wide varieties of igneous rocks are extensively utilized as stones for decoration purposes and as a potential source for building. With the use of petrological (mineralogical and chemical) and physico-mechanical analyses, the current work accurately mapped the Dokhan Volcanics (DV) and utilized them as decorative stones and their prospective in building materials using Frattini's test. Field observations indicate that metavolcanics, DV, and monzogranites are the principal rock units exposed in the studied area. The DV rocks are characterized by a dense series of stratified, rhyolitic to andesitic lava interspersed with a few pyroclastics. Andesite, andesite porphyry, dacite, and rhyolite are the primary representatives of the selected DV. The lack of infrequent appearance of mafic units in the current volcanic eruptions indicates that the primary magma is not mantle-derived. This is supported by their Mg# (17.86–33.57). Additionally, the examined DV rocks have Y/Nb ratios above 1.2, suggesting a crustal source. The role of fractionation is interpreted by their variation from andesite passing through dacite to rhyolite, which is indicated by gradual negative distribution groups between silica and TiO_2, Fe_2O_3, CaO, MgO, Co, and Cu from andesite to rhyolitic lava. Additionally, a wide range of widely used DV rocks like Y/Nb, Rb/Zr, and Ba/Nb point to crustal contamination in the rhyolitic rocks. The partial melting of the lower crust can produce andesitic magma, which ascend to higher crustal levels and form lava of calc-alkaline. A portion of this lava may split, settle at shallow crustal depths, and undergo differentiation to create the DV rocks. Based on the results of physico-mechanical properties, the studied samples met the requirements for natural stone to be used as decorative stones, whether as interior or exterior installations. The pozzolanic assessment of the studied rocks revealed their usability as supplementary cementitious materials in the building sector.

Keywords: Dokhan volcanics; geochemistry; physico-mechanical properties; decorative stones; building materials

Citation: Lasheen, E.S.R.; Sami, M.; Hegazy, A.A.; Arman, H.; Sanislav, I.V.; Ahmed, M.S.; Rashwan, M.A. Petrological Characteristics and Physico-Mechanical Properties of Dokhan Volcanics for Decorative Stones and Building Material Applications. *Buildings* **2024**, *14*, 3418. https://doi.org/10.3390/buildings14113418

Academic Editors: Jianyong Han, Xiaoyu Bai and Nan Yan

Received: 25 September 2024
Revised: 8 October 2024
Accepted: 23 October 2024
Published: 27 October 2024

1. Introduction

The western edge of the Arabian–Nubian Shield (ANS) is made up of the Precambrian rocks found in the Eastern Desert and Sinai [1]. The East African Orogen led to the evolution

of the Precambrian ANS rocks "(900–540 Ma)" [2]. The Earth's juvenile crust, with the biggest expanse, is represented by the ANS. The post-collisional volcanic activities with varying intrusive granitic rocks, ophiolites, and accreted arc associations are the ANS' main constituents. As the Ocean of Mozambique closed and East and West Gondwana merged, accretion occurred. The Red Sea rifting caused an uplift along its shoulders, producing exceptional Precambrian exposures on the eastern sector of Saudi Arabia and the western side of Egypt [3,4]. It was at 540 Ma that the ANS reached tectonic stability.

The Precambrian rocks were formed through three stages comprising (a) subduction, (b) arc accretions, and (d) post-collisional accumulations [5,6]. The last stage is segmented by Dokhan Volcanics (DV), deposits of Hammamat, and pink to white granites. Three categories of volcanic rocks can be distinguished in the Precambrian rocks: DV; younger; and older metavolcanics. The latter are frequently linked to basaltic ophiolitic rocks, whether they originate from the suprasubduction zone or Mid-Ocean Ridge. Conversely, the arc setting is associated with the rhyolitic to basaltic younger. Both the Central and Southeastern Deserts of Egypt are rich in both previous types. In contrast, the DV (615–560 Ma) rocks, which are unmetamorphosed, have a K value between medium and high, are commonly rhyolitic to andesitic with the widespread occurrence of welded tuffs and extensively distributed in the Northeastern Desert and Sinai [2,7–12] (Figure 1). There are disagreements on the setting and petrogenesis of the DV, and there are several disagreements concerning the sources, tectonic setting, and other events that shaped the history of these rocks. They may be emplaced in (a) compression regime [7,13], (b) crustal accumulation (extension) [14,15], and (c) transition stage between the previous two settings [16,17]. Field relationships show that the DV precede the younger granites, but they are postdated by older granites [9,10,16].

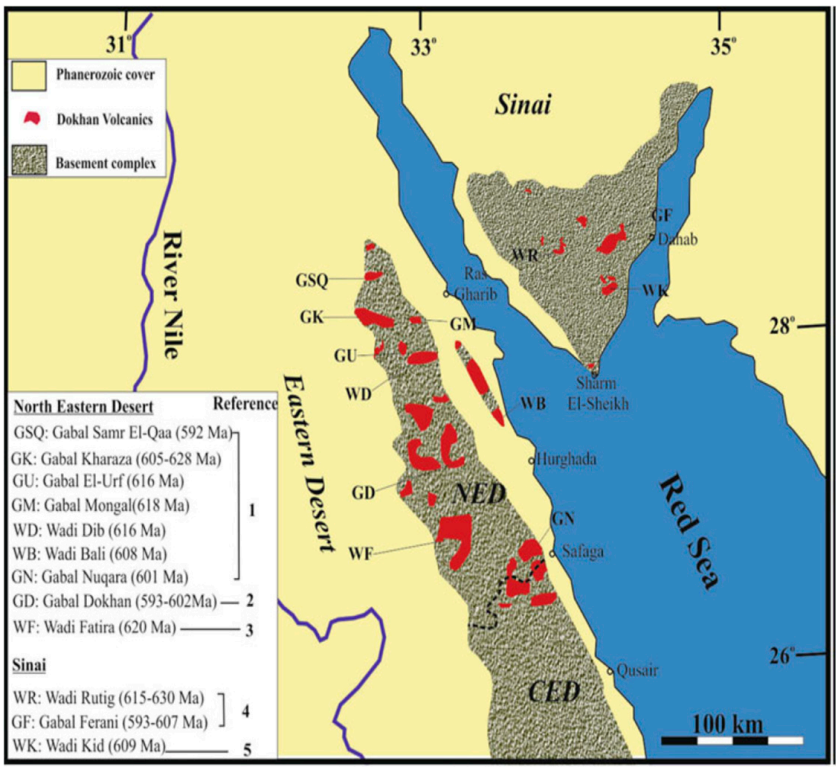

Figure 1. Dokhan volcanic distribution map, Egypt [7].

Any natural stones, whether igneous (volcanic, plutonic), sedimentary, or metamorphic, can be used as decorative or ornamental stones, providing they achieve some parameters such as the ability to be cut into specific sizes or shapes, compactness, durability, in addition to the aesthetic appearance. Therefore, for a long time, ancient cultural projects

and historical landmarks, including pyramids, palaces, and old historical cities, involved the significant utilization of natural stones as building materials [17–23]. Additionally, they have been used for other construction purposes such as building facing, curbing, monuments, paving stones, and others [18,24].

The majority of natural stones used as decorative or ornamental stones fall under two main groups; the first is called the siliceous stones group, encompassing, for example, granite, basalt, gneiss, gabbro, and diorite, while the second group is called carbonaceous stones, comprising, for example, marble, limestone, and onyx [25–28]. During the last 10 years and with the continuous increase in the world population growth rates, there was a remarkable expansion in the urban development projects that led to the increasing demand for the production of building materials, and one of them is dimension stone for decorative purposes [29,30]. Therefore, in 2017, about one hundred fifty million tons of dimension stones were produced by 27 countries worldwide [31]. The majority of this production (about 72%) was shared by Italy, China, Turkey, Iran, and India [32,33].

Regarding the availability and world share of Egyptian natural stones, throughout the nation, there are over fifty different categories of natural stones that are eligible to be utilized as ornamental stones [34,35], with a production volume reaching about 5.25 million tons annually, representing around 4% of world sharing [30]. In terms of dimension-stone production, Egypt was ranked seventh [27,29,36].

The huge worldwide distribution of natural stones of aesthetic appearance with a difference in their chemical and mineralogical composition attracted the attention of researchers from ancient times to the present for studying their performance and suitability for decorative purposes in construction sectors [20,21,27,37–40].

All these studies focused on the granitoid rocks with different types, such as monzogranites, syenogranite, alkali-feldspar granites, albitized granites, and granodiorite being the most common and widespread igneous rocks. Few studies have investigated the suitability of basalt, being the commonest volcanic rocks, as construction and building materials. Agasnalli et al. [41] studied the physical and mineralogical properties of two types of igneous rocks (basalt and granite) to assess their suitability as building materials. They found that basalt in the aggregate form was most demanded in the construction sector due to its interesting very low water absorbability, hardness, compactness, durability, and availability at affordable prices. Sivanandhini et al. [42] investigated the suitability of using basalt rock as aggregates in building construction. The characterization of basalt aggregates showed a higher strength under impact load than normal aggregates, high specific gravity, low water-absorption capacity, and high resistance against abrasion. All these features enabled the basalt aggregates to be used extensively as an engineering material in the construction of airfield pavement roads, concrete and asphalt mixes, and railroad ballast.

Other researchers utilized the wastes of the natural stone industry as alternative materials for aggregates or even cement binders in the building materials and construction sector. Regardless of whether plutonic or volcanic, mafic igneous rocks (such as gabbro and basalt) are primarily used as an alternative source of aggregates for the production of concrete [43–48]. The utilization of these types of rock was based on their distinctive properties, such as low absorption, high density, and resistance to abrasion, in addition to their chemical resistance compared with other aggregate types [45,46]. Furthermore, many other works dealt with powders of some natural stones such as basalt, andesite, metagabbro, and granite as an additional cement-making ingredient binder in cement mortar and concrete products [49–58]. The additional materials, whether with a cementitious or filling effect, were commonly used as alternative materials with variable proportions for cement or fine aggregate in cement products to increase their resilience to unfavorable attack circumstances [54,56].

On the other hand, the Ordinary Portland cement industry is considered one of the main carbon dioxide-emitting industries, with an estimated 7% of global carbon dioxide emissions [59]. One of the routes to mitigate the carbon footprint of cement production is the usage of Pozzolanic materials. These materials are usually mineral admixtures,

aluminous or siliceous materials that have no or very little cementitious ability. However, when it splits finely and is combined with water, it reacts with calcium hydroxide at room temperature to create substances that have cementitious qualities. The pozzolanic materials are usually blended with cement or added to Portland clinker during the grinding process [60].

Natural rocks such as pumice, tuff, diatomite, volcanic glass/ash, clay, and laterite are reported as natural pozzolans [61]. The advantages of applying these materials as cement additives in concrete products are the reduction in production costs, the energy consumed in cement production, and the enhancement of various concrete properties such as durability and physical and mechanical characteristics.

Laibao et al. [52] recorded a delay in the setting times and hydration process with the addition of basalt powder, in addition to a trivial negative effect on compressive strength. According to Labbaci et al. [51], the using of volcanic rock powders such as basalt, andesite, and scoria up to 30% exhibited high pozzolanic activity, in addition to their resistance to chemical attack conditions compared to cement. Ghorbani et al. [50] reported an insignificant effect on the physical and mechanical properties of concrete using up to 20% granite dust. Moreover, a higher resistance toward sulfate and chloride attack was observed. According to Rashwan et al. [56], using up to 15% of metagabbro improved the physico-mechanical properties of cement pastes. Furthermore, an enhancement in several types of chemical attacks was also reported.

2. Study Significance

Despite all the previous studies that dealt with the characterization of natural stones as dimension stones for decorative and building purposes, there is a lack of information on using volcanic rocks as ornamental stones. Along the same line, volcanic rocks of different types, such as basalt, andesite, and dacite, have attracted the attention of many researchers worldwide for their use as supplementary cementitious materials in mortar and concrete [62–67]. However, no attempts have been made to investigate the pozzolanic activity of volcanic rocks at Gabal El Dokhan, Egypt, despite the great areas they cover.

The choice of this study area results from the diversities of their rock units, which range from acidic (rhyolite) to intermediate (dacite, andesite), which are characterized by compactness and hardness, in addition to their wide extension. The hardness (high compressive strength), compactness (low porosity and high durability), and fineness (rapid cooling and a chance for active silica) are the main parameters that should be achieved in the dimensions and building stones. Therefore, the present study evaluates the Dokhan volcanics rocks' suitability for usage in the construction sector as decorative stones and their perspective as natural pozzolana in building materials. The evaluation requires physico-mechanical investigation, in addition to pozzolanic assessment using standard test methods and comparing the results with the international specifications. The novelty of this research is that it is the first study that reports new physical and mechanical properties on the Dokhan volcanics at Gebel Dokhan, NED, as well as new petrographic features, major, and trace composition to deduce their setting and petrogenesis. The use of volcanic rocks as a supplementary cementitious material in building and construction sectors can add an environmental benefit by reducing carbon dioxide emissions from the cement industry.

3. Field Geology

The researched location is situated in the NED of Egypt (Figure 2a), some 50 km northwest of the city of Hurghada. Field observations indicate that metavolcanics, DV, and monzogranites are the principal rock units exposed in the studied area (Figure 2b,c). Numerous dykes with varying compositions that primarily trend NE–SW, NNE–SSW, and NNW–SSE divide all of these rock units. A large portion of the mapped region is covered by the DV (1705 m a.s.l.) (Figure 3a,b). This area is distinguished by its rough terrain, crenulated summits, and gentle to deep slopes. The DV in the region have narrowly spaced joints and are broken. They have a distinct layer that suggests a series of explosions. Sharp

and sporadic intrusive interactions allow syenogranites to infiltrate them (Figure 3c). They are characterized by a dense series of stratified, rhyolitic to andesitic lava interspersed with a few pyroclastics [11]. They occur in sheets and are typically distinguished by columnar jointing. Numerous faults cut through them, creating a unique rocky terrain, and numerous small Wadis run through these rocks. The DV rocks are large and hard, and their colors vary from pink to brownish red to crimson in acidic types. When they are chloridized, the intermediate rocks turn from grey to dark grey or green. While basaltic rocks are rare, andesite, dacite, and rhyolite are the most common types of DV rocks. These rocks are mostly invaded by acidic dikes (Figure 3d).

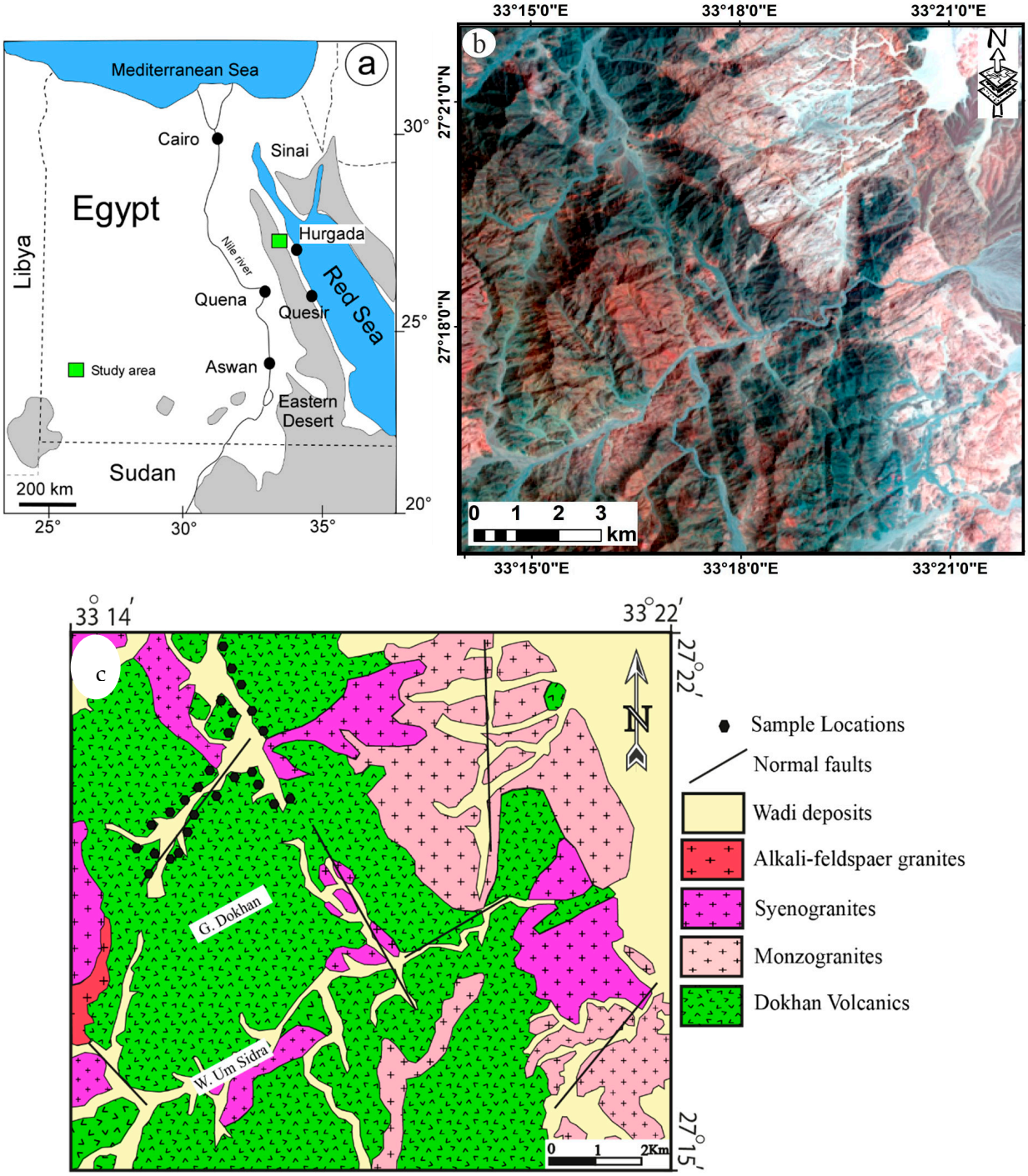

Figure 2. (**a**) Location map of the Gebel Dokhan area; (**b**) Landsat image of Gebel Dokhan area; (**c**) Geological map of Gebel Dokhan area [11].

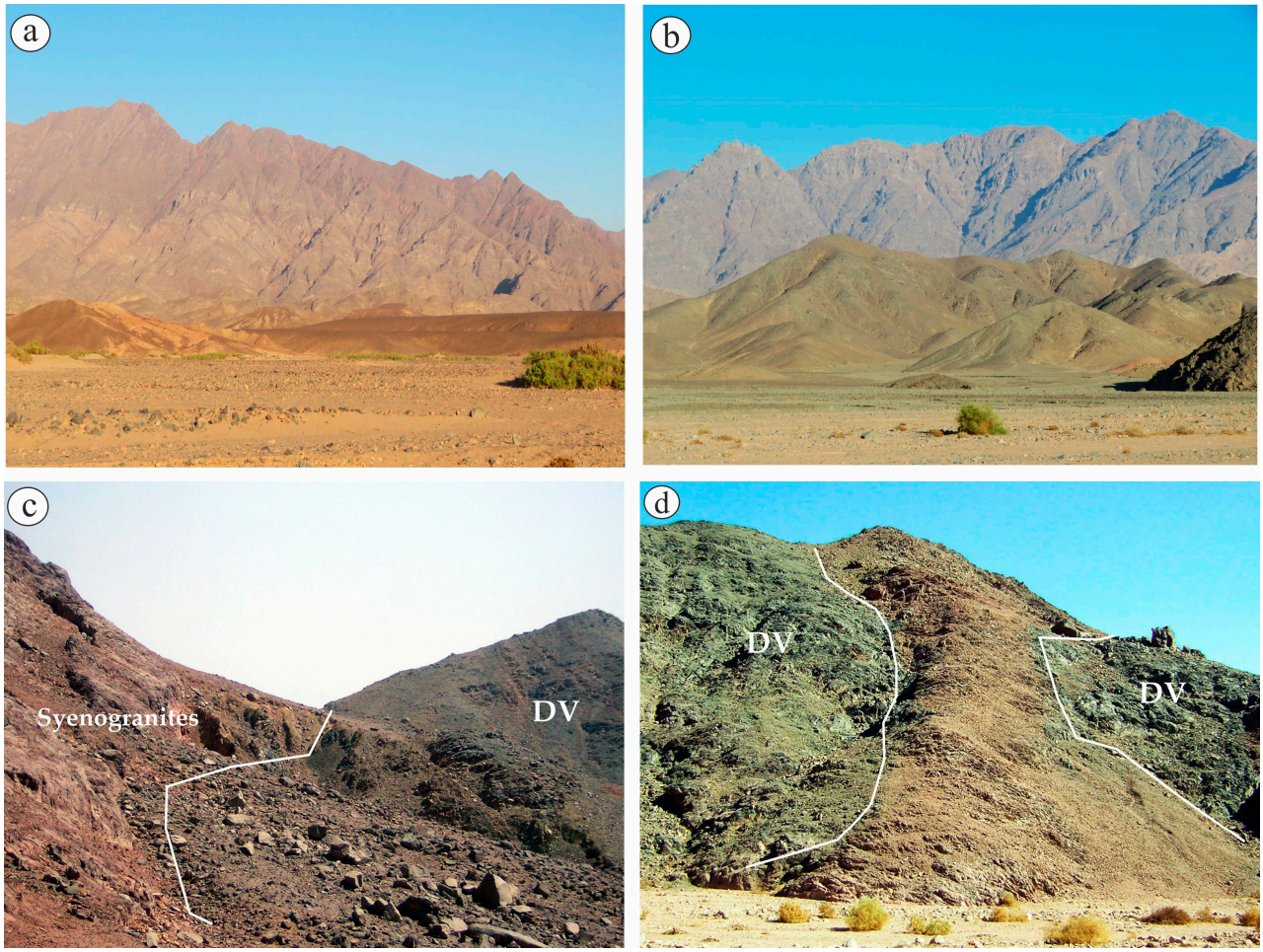

Figure 3. Field photographs of Dokhan volcanics (DV): (**a**,**b**) General view of G. El Dokhan volcanics; (**c**) Syenogranites intruding Dokhan volcanics; and (**d**) Acidic dike injected the Dokhan volcanic rocks.

4. Methodology

4.1. Petrological Study

Nineteen specimens were procured at the reference location of Gebel Dokhan. In the Rocks Lab (Al-Azhar University), fifteen representative samples are thin-sliced, and a polarizing microscope is used to determine the preliminary mineralogy and their relationships. As the classification of igneous rocks as well as determination of their tectonic settings basically depended on their chemical composition, fifteen samples were pulverized to less than 75 µm size and then subjected to chemical analysis using the XRF technique (X-ray Fluorescence Axios, PANalytical 2005). The detection of element concentrations was carried out with a Sequential WD-XRF Spectrometer using a standard guide for elemental analysis (ASTM E-1621) [68] by wave-length-dispersive X-ray fluorescence Spectrometer. The Loss on Ignition (LOI) was measured according to the standard test method ASTM D-7348 [69]. The measurements were carried out at the National Research Centre in Egypt.

4.2. Physico-Mechanical Tests

The evaluation of natural stones to determine their suitability as dimension decorative stones depends on some important parameters called physical and mechanical properties according to (ASTM C615) These properties, which include water absorption, density, compressive strength, and abrasion resistance, determine the hardness and durability of dimension stones under various conditions (loads, abrasion, and wetting) of interior or exterior applications. All physical and mechanical measurements are carried out in the Marble and Granite Testing Laboratory (MGTL) at the National Research Centre in Egypt.

Therefore, the DV rocks were prepared into cubic samples measuring 50 × 50 × 50 mm and rectangular samples measuring 50 × 50 × 25 mm. These dimensional samples were subjected to mechanical and physical properties (Figure 4). The primary physical characteristics comprise the water absorption and bulk density according to (ASTM C97) [70] and apparent porosity according to (EN 1936) [71]. According to these standard methods, the samples were dried in an oven at around 60 °C until the constant mass was attained, in accordance with these test procedures.

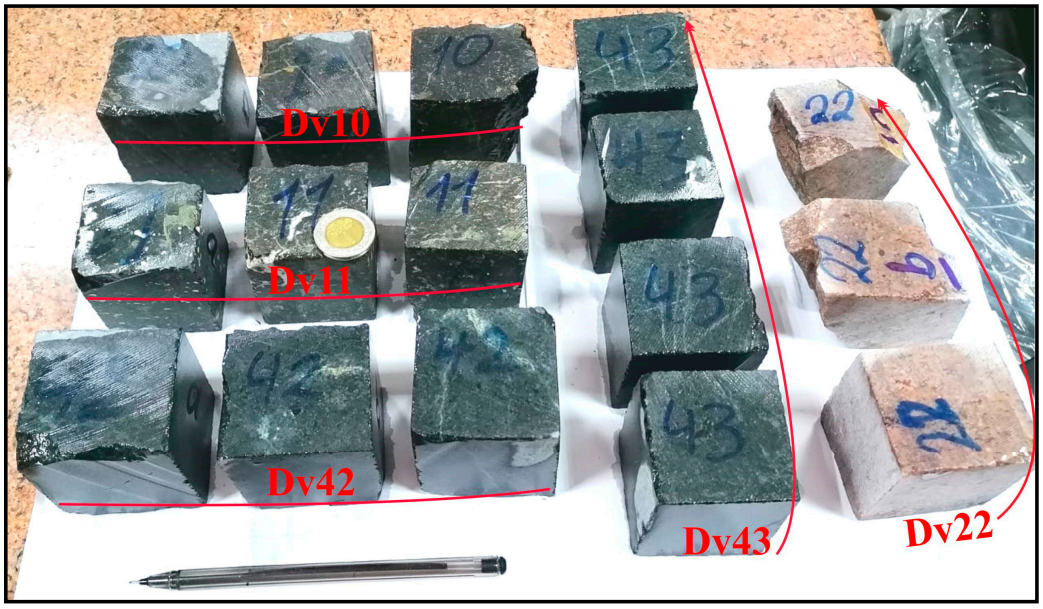

Figure 4. Photograph showing cubic specimens of different types of Dokhan volcanics.

Following their removal from the water bath, the saturated samples' surfaces were dried with a dumped cloth, and the weight of the saturated-surface-dry (SSD) sample was recorded to the closest 0.01 g. Following that, they were submerged in water, and the weight they were suspended in was calculated to the closest 0.01 g.

The water absorption, apparent porosity, dry bulk density, and saturate-surface-dry bulk density were calculated according to the following equations:

$$\text{*Water absorption, \%} = 100 \times (\text{SSD weight} - \text{Dry weight})/\text{Dry weight} \quad (1)$$

$$\text{*Apparent porosity, \%} = 100 \times (\text{SSD weight} - \text{Dry weight})/(\text{SSD weight} - \text{Suspended weight}) \quad (2)$$

$$\text{*Dry Bulk density, kg/m}^3 = 1000 \times \text{Dry weight}/(\text{SSD weight} - \text{Suspended weight} \quad (3)$$

$$\text{*SSD Bulk density, kg/m}^3 = 1000 \times \text{SSD weight}/(\text{SSD weight} - \text{Suspended weight}). \quad (4)$$

These characteristics measure the ability of rocks to withstand the deleterious matters that may penetrate through the rock pores and affect their durability.

The mechanical properties, which include the compressive strength test according to (ASTM C170) [72] and abrasion resistance test according to (ASTM C241) [73], measure the durability of rocks against loads and frictions, especially when used in the floors of the exterior installations. According to these methods, the prepared samples were fully dried in a ventilated oven at around 60 °C until they reached constant mass. Regarding the compression test, the loading areas of the test samples were determined to the nearest 0.1 mm^2; after that, the samples were centered between the upper and lower plates, and the load was applied at a rate of 0.5 MPa/s. until reaching the failure load. The compressive strength is computed using the following equation:

$$\text{*Compressive strength, MPa} = \text{Total load (N)}/\text{Loading area (mm}^2) \quad (5)$$

Regarding the abrasion resistance test, the prepared specimens were subjected to two types of abrasion tests. In the first type, the prepared specimens were abraded for 225 revolutions at a rate of 45 rpm using an abrasive material (white fused alumina) under 19 N (2 kg) load according to [73]. The values of abrasion resistance or abrasive hardness (Ha) of each specimen can be calculated as follows:

$$*\text{Ha} = 10.95\text{G}\ (2000 + \text{Ws})/2000 * \text{Wa} \quad (6)$$

where "G" is the bulk specific gravity of the sample; "Ws" is the average weight of the specimen (original weight plus final weight divided by 2), g, and "Wa" is the loss of weight during the grinding operation, g.

The second type of abrasion test is based on the Wide Wheel test [74]. In this test, the specimens were abraded for 75 revolutions in 60 sec using fused alumina (80 grit) under 137 N (14 kg) load. The value of abrasion resistance is expressed as the width (in mm) of the resulting groove.

4.3. Pozzolanic Activity Assessment

The literature categorizes pozzolanic material classification tests into two primary types. The first class directly assesses pozzolanic activity by measuring the consumed calcium hydroxide during the reaction with the test material. The Frattini test method is a prominent example in this category and is mainly used inBS EN 196-5 [75]

The second class employs an indirect method, evaluating pozzolanic activity through comparative analysis of compressive strength. This involves comparing neat mortar with mortar containing the test pozzolan at various hydration periods to determine the strength activity index (SAI) according to ASTM C618 and ASTM C311 [76,77].

In this article, the Frattini test method, according to [75], was used to assess the pozzolanic activity of the samples as it provides insights about the pozzolanic activity without the interference of other factors like packing that can influence the strength activity index (SAI).

5. Results and Discussion

5.1. Petrography

Andesite, andesite porphyry, dacite, and rhyolite are the primary representatives of the selected DV. The majority of these volcanics are porphyritic, with phenocrysts making up between 25 and 70 percent of the entire rock mass. Both andesite (DV43) and its porphyry (DV11) have a porphyritic texture (Figure 5a,b), with the latter showing sporadic cumulophyritic (Figure 5b) textures (with plagioclase phenocrysts reaching up to 70%). The primary phenocrysts in a fine-grained groundmass are hornblende and plagioclase. About 25–30 percent of the lava is made up of andesine (An32–41) phenocrysts that are euhedral to subhedral, carlsbad, zoned (Figure 5c), and tabular. Occasionally, they are fractured, saussuritized, epitodized, or kaolinitized. Therefore, their twins partially or completely disappear. The lava contains roughly 10% modal percent hornblende phenocrysts. The primary accessory is opaques; the secondary minerals include saussurite, chlorite, and epidote. In a fine-grained groundmass, dacite (DV42 and 10) is composed of phenocrysts of biotite and oligoclase ($An_{22–28}$). The majority of oligoclase is fresh (Figure 5d), lamellae, carlsbad (Figure 5e), and pericline twinning; however, it can occasionally be slightly/completely epitodized (Figure 5f). Chlorite is entirely changed from flak phenocrysts that biotite generates (Figure 5g). Typical accessories include iron oxides and titanite. Secondary minerals include epidote, kaolinite, and chlorite. In a finely obtained groundmass, rhyolites (DV22) have quartz and platy K-feldspar phenocrysts along with small plagioclase phenocrysts. Quartz is an elongated equant and is widespread in the groundmass as fine grains. Some crystals have a definite extinction. K-feldspar phenocrysts are mostly orthoclase perthite with flamy worm texture (Figure 5h) and turbid surface pointing to kaolinitization processes (Figure 5i). Commonly, they are fractured and engulfing plagioclase. Secondary minerals include kaolinite, chlorite, and sericite; accessories include hematite, apatite, and zircon.

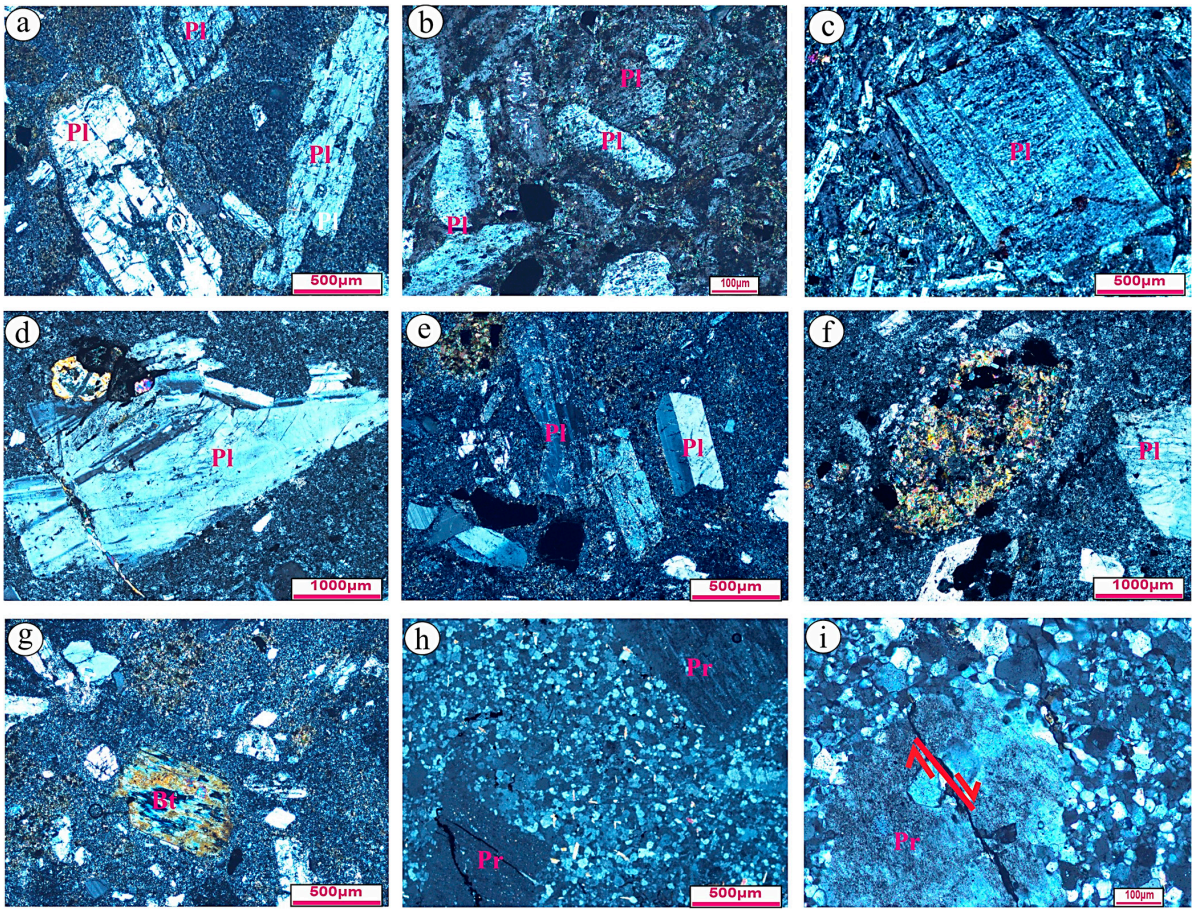

Figure 5. DV photomicrographs displaying the following: (**a**) fractured phenocrysts of plagioclase, andesite (DV43); (**b**) laths of plagioclase producing cumulophyritic texture, andesite porphyry (DV11); (**c**) euhedral plagioclase phenocrystal embedded in fine-sized plagioclase, andesite porphyry (DV11); (**d**) fractured filled by sericite of fish head-shaped of plagioclase, dacite (DV10); (**e**) fresh carlsbad and slightly altered plagioclase phenocrysts embedded in groundmass, dacite (DV42); (**f**) completely epitodized plagioclase phenocrystal, dacite (DV10); (**g**) chloritized biotite phenocrystal embedded in groundmass, dacite (DV10); (**h**) flamy perthite phenocrysts embedded in felsic groundmass, rhyolite (DV22); and (**i**) turbid perthite phenocrystal enclosing zoned and dislocated plagioclase crystal, rhyolite (DV22).

5.2. Petrochemistry

5.2.1. Classification and Lava Variations

DV analysis (major and trace elements) displays variation in their composition (Table 1). Several proposed diagrams classify the variety of DV rocks. In terms of the TAS binary diagram [78], the rocks of DV straddle the rhyolite, dacite, and andesite (andesite and andesite porphyry) fields (Figure 6a). On the Zr/TiO_2-SiO_2 diagram [79], rhyolite, dacite, and both andesite and andesite porphyry lie within the fields of rhyolite, dacite, and andesite, respectively (Figure 6b). The older volcanics are distinguishably basaltic andesite with low-K basalts. Like the DV, the younger volcanics span a broad range of SiO_2, but they differ in that they are low- to medium-K. The DV rocks are commonly medium-K to high-K. The examined rocks are sub-alkaline, their maximum value of agpaitic index is less than 0.84, pointing to non-alkaline nature. Their alkalinity can be further identified by Irvin and Barger [80] (Figure 6c) and Le Maitre [81] with a SiO_2-K_2O diagram; the examined DV rocks are plotted in medium-K and high-K calc-alkaline (rhyolite) suites (Figure 6d). Diverse parameters of the DV analysis are used to differentiate adakites (of both low and high silica) from other calc-alkaline [82]. The examined DV rocks are normal arc rocks rather than adakites due to low Y (9.45–16) and Sr/Y (5.07–34.3) contents. This is supported by SiO_2-Sr/Y (Figure 6e); the examined DV samples are non-adakites and plotted in the arc field [82].

Table 1. Whole rock analysis of the Dokhan volcanics, G. El Dokhan, Northeastern Desert, Egypt.

Dv No.	42a	42b	42c	43a	43b	43c	10a	10b	10c	22a	22b	22c	11a	11b	11c
SiO_2	63.73	63.50	62.98	61.40	60.47	60.09	65.68	65.11	64.84	75.51	73.26	74.39	61.70	60.36	60.23
TiO_2	0.60	0.80	0.70	0.62	0.71	0.73	0.45	0.51	0.53	0.12	0.17	0.15	0.56	0.54	0.65
Al_2O_3	16.73	16.78	16.36	16.94	16.26	16.45	15.70	16.04	16.17	13.71	14.82	14.26	15.12	16.03	15.58
Fe_2O_3	4.95	5.23	5.09	5.35	5.71	6.03	4.41	5.06	4.98	1.02	1.31	1.16	6.37	6.97	6.17
MnO	0.09	0.11	0.10	0.10	0.12	0.11	0.09	0.10	0.09	0.07	0.09	0.08	0.20	0.24	0.22
CaO	3.45	4.01	3.73	4.14	4.79	4.46	2.68	3.04	2.91	0.40	0.48	0.44	3.30	3.81	3.55
MgO	2.37	2.36	2.36	2.69	2.67	2.68	2.15	2.14	2.15	0.28	0.28	0.28	3.13	3.11	3.12
K_2O	1.71	2.09	1.90	1.19	1.45	1.32	2.12	2.59	2.35	3.20	4.01	3.60	1.52	1.84	1.68
Na_2O	4.64	4.48	4.56	4.43	4.27	4.35	4.66	4.51	4.58	4.84	4.74	4.79	3.90	3.76	3.83
P_2O_5	0.58	0.46	0.52	0.62	0.49	0.56	0.55	0.44	0.49	0.06	0.05	0.06	0.45	0.36	0.41
LOI	0.76	0.76	0.76	1.70	1.70	1.70	1.10	1.10	1.10	0.40	0.40	0.40	3.33	3.33	3.33
Normative values															
Qz	20.87	18.63	19.11	19.97	17.27	17.77	23.09	20.49	21.13	34.06	29.06	31.56	22.74	19.70	20.42
C	2.34	0.94	1.24	2.33	0.15	1.09	2.18	1.33	1.96	1.72	1.94	1.83	2.15	1.79	1.97
Or	10.12	12.32	11.22	7.03	8.54	7.79	12.50	15.30	13.90	18.89	23.72	21.30	8.97	10.86	9.91
Ab	39.29	37.93	38.61	37.48	36.12	36.80	39.41	38.17	38.79	40.94	40.08	40.51	33.02	31.78	32.40
An	13.36	16.92	15.14	16.46	20.53	18.50	9.74	12.24	11.23	1.55	2.03	1.79	13.41	16.57	14.99
Hy	5.91	5.87	5.89	6.70	6.65	6.68	5.36	5.34	5.35	0.70	0.71	0.70	7.80	7.75	7.77
Il	0.20	0.24	0.22	0.22	0.26	0.24	0.18	0.22	0.20	0.16	0.19	0.17	0.43	0.51	0.47
Hm	4.95	5.23	5.09	5.35	5.71	6.03	4.41	5.06	4.98	1.02	1.31	1.17	6.38	6.97	6.17
Ru	0.50	0.68	0.59	0.51	0.58	0.60	0.36	0.39	0.43	0.04	0.07	0.06	0.34	0.28	0.41
Ap	1.37	1.08	1.23	1.48	1.17	1.32	1.30	1.04	1.17	0.15	0.12	0.14	1.07	0.85	0.96
Sum	98.91	99.85	98.34	97.53	96.98	96.81	98.51	99.57	99.14	99.23	99.22	99.23	96.30	97.04	95.47
Trace elements (ppm)															
As	18.50	18.00	18.25	5.70	5.80	5.75	13.10	13.00	13.05	45.40	45.87	45.64	3.30	3.56	3.43
Ba	443.00	441.00	442.00	384.20	382.00	383.10	542.10	540.60	541.35	298.20	301.00	299.60	606.10	605.00	605.55
Cd	8.80	8.22	8.51	6.20	5.98	6.09	7.80	7.91	7.86	4.00	3.99	4.00	5.80	5.21	5.51
Ce	57.30	57.22	57.26	32.90	31.98	32.44	57.10	56.91	57.01	24.50	23.99	24.25	29.50	30.01	29.76
Co	19.10	20.01	19.56	32.60	31.56	32.08	21.30	20.91	21.11	18.50	17.88	18.19	31.90	30.41	31.16
Cr	12.80	12.55	12.68	16.00	15.09	15.55	21.70	20.93	21.32	3.30	3.11	3.21	11.90	10.97	11.44
Cs	2.80	2.22	2.51	4.70	2.61	3.66	ND	ND	ND	7.40	6.87	7.14	10.30	9.55	9.93
Cu	6.40	6.03	6.22	6.40	5.94	6.17	5.10	4.65	4.88	3.70	2.95	3.33	5.70	4.87	5.29
Ga	23.00	23.06	23.03	24.10	24.05	24.08	21.90	21.09	21.50	15.50	14.76	15.13	20.90	21.01	20.96
Hf	3.20	2.83	3.02	12.30	11.05	11.68	19.80	18.99	19.40	ND	ND	ND	12.10	11.43	11.77
La	25.90	24.06	24.98	13.80	12.03	12.92	33.30	31.22	32.26	21.10	20.89	21.00	21.20	20.85	21.03
Nb	1.60	1.03	1.32	0.90	0.08	0.49	3.30	2.91	3.11	4.50	4.25	4.38	1.50	1.23	1.37
Nd	21.60	20.75	21.18	12.30	10.86	11.58	34.60	34.11	34.36	17.40	15.88	16.64	9.40	9.21	9.31
Ni	5.90	4.87	5.39	8.00	7.54	7.77	10.30	9.88	10.09	1.10	1.02	1.06	8.70	7.93	8.32
Pb	25.70	24.54	25.12	23.70	22.64	23.17	34.90	33.74	34.32	22.00	21.07	21.54	27.70	26.04	26.87
Rb	36.30	35.02	35.66	27.40	27.01	27.21	50.20	51.00	50.60	82.40	82.02	82.21	52.30	53.00	52.65
Sc	11.10	10.54	10.82	13.50	12.05	12.78	8.30	7.88	8.09	2.20	2.02	2.11	12.30	11.29	11.80
m	5.90	6.11	6.01	7.60	6.98	7.29	ND	ND	ND	8.00	9.52	8.76	10.60	10.41	10.51
Sn	50.30	50.82	50.56	51.00	50.67	50.84	61.40	60.82	61.11	10.90	11.52	11.21	50.90	51.03	50.97
Sr	496.80	495.00	495.90	432.20	433.00	432.60	302.30	303.00	302.65	50.70	51.77	51.24	425.60	423.00	424.30
Th	17.50	17.01	17.26	18.60	19.00	18.80	23.30	23.53	23.42	9.80	8.67	9.24	16.80	15.32	16.06
V	33.40	32.43	32.92	37.00	38.00	37.50	35.50	35.22	35.36	ND	ND	ND	69.70	68.54	69.12
Y	16.00	15.32	15.66	12.60	13.00	12.80	14.80	14.06	14.43	10.00	9.45	9.73	13.10	12.38	12.74
Zn	54.30	55.01	54.66	65.80	66.01	65.91	50.10	51.01	50.56	29.80	30.40	30.10	241.80	244.00	242.90
Zr	147.10	146.87	146.99	131.20	132.00	131.60	183.10	184.00	183.55	131.50	130.80	131.15	147.10	146.70	146.90
Geochemical Parameters															
Agpaitic	0.57	0.57	0.59	0.51	0.53	0.52	0.63	0.64	0.62	0.83	0.82	0.83	0.53	0.51	0.52
Sr/Y	31.05	32.31	31.67	34.30	33.31	33.80	20.43	21.55	20.97	5.07	5.48	5.27	32.49	34.17	33.30
Th/Zr	0.12	0.12	0.12	0.14	0.14	0.14	0.13	0.13	0.13	0.07	0.07	0.07	0.11	0.10	0.11
Rb/Zr	0.25	0.24	0.24	0.21	0.20	0.21	0.27	0.28	0.28	0.63	0.63	0.63	0.36	0.36	0.36
La/Sm	4.39	3.94	4.16	1.82	1.72	1.77	ND	ND	ND	2.64	2.19	2.40	2.00	2.00	2.00
Y/Nb	10.00	14.87	11.91	14.00	162.50	26.12	4.48	4.83	4.65	2.22	2.22	2.22	8.73	10.07	9.33
Ba/Nb	276.88	428.16	336.12	426.89	4775.00	781.84	164.27	185.77	174.35	66.27	70.82	68.48	404.07	491.87	443.63
K/Rb	471.90	595.37	532.53	434.31	534.99	484.29	421.31	507.65	464.82	387.86	489.27	438.45	290.25	346.60	318.61
Mg#	32.37	31.07	31.71	33.46	31.87	30.78	32.80	29.76	30.12	21.55	17.86	19.52	32.95	30.84	33.58

Among the studied lava, rhyolite has high SiO_2 (avg. 74.39 wt%), alkalis (avg. 8.39 wt%), As (avg. 45.64 ppm), Nb (avg. 4.38 ppm), and Rb (avg. 81.21 ppm), but less much in TiO_2 (avg. 0.15 wt%), Al_2O_3 (avg. 14.26 wt%), Fe_2O_3* (avg. 1.16 wt%),

CaO (avg. 0.44 wt%), MgO (avg. 0.28 wt%), Ba (avg. 299.6 ppm), Cr (avg. 3.21 ppm), Cu (avg. 3.33 ppm), Co (avg. 18.19 ppm), Ni (avg. 1.06 ppm), and Sr (avg. 51.24 ppm), reflecting highly fractionated rocks. In contrast, the andesite porphyry rocks have noticeable enrichment of Fe_2O_3* (avg. 6.51 wt%), MgO (avg. 3.12 wt%), LOI (avg. 3.233 wt%), Ni (avg. 8.32 ppm), Ba (avg. 605.55 ppm), Sr (avg. 424.3 ppm), and Zn (avg. 243 ppm), suggesting to be less fractionated with abundant plagioclase minerals. In comparison to N-MORB (Figure 6f), all the DV samples display enrichment in Ba, Rb, Pb, and K, but much depletion in Ti and Nb, besides Sr and P in rhyolite (as a result of fractionation of iron oxides, feldspar, and apatite). Such DV rocks with subduction-related calc-alkaline are generally characterized by these geochemical characteristics [10,83].

5.2.2. Tectonic Emplacement

Regarding the DV environment, there is disagreement, with theories suggesting a subduction-related regime [7,10], an extension regime [84], or a zone of transition from subduction to extension [2,9]. The DV, which date from 600 to 590 Ma, erupted during the period between collision and extension. The geochemical characteristics show that the DV rocks are not linked to A-type intrusions [2,9]. All of the DV rocks have a calc-alkaline, Ti and Nb negative anomalies and an enrichment of LFS elements in comparison to HFS elements, yielding a signature of subduction setting. Immobile trace (Nb, Ti, Zr, and Y) elements are extensively employed to distinguish between various DV settings. The intermediate DV samples straddle the calc-alkaline basalt and Dokhan volcanic field, while rhyolite lies near this field using ternary Zr-Ti/100-Sr/2 (Figure 7a) diagram [85], implying a convergent setting. Additionally, all samples lie within the VOLG field according to the Nb+Y-Rb (Figure 7b) diagram [86]. All samples of DV plot in the destructive plate (arc basalt) according to the ternary tectonic Th-Hf-Nb (Figure 7c) diagram [87].

Additionally, the examined DV eruptions occurred in a continental rather than an oceanic environment depending on the P_2O_5-K_2O-TiO_2 (Figure 7d) diagram [88], similar to those of Eliwa et al. [9]. These rocks are straddling the volcanic arc rather than within the plate and transition zone depending on Nb-SiO_2 (Figure 7e) [89]. Therefore, instead of being created in a post-collisional context, the DV rocks were likely placed in a subduction-related context, which is a continental arc of thicker crust.

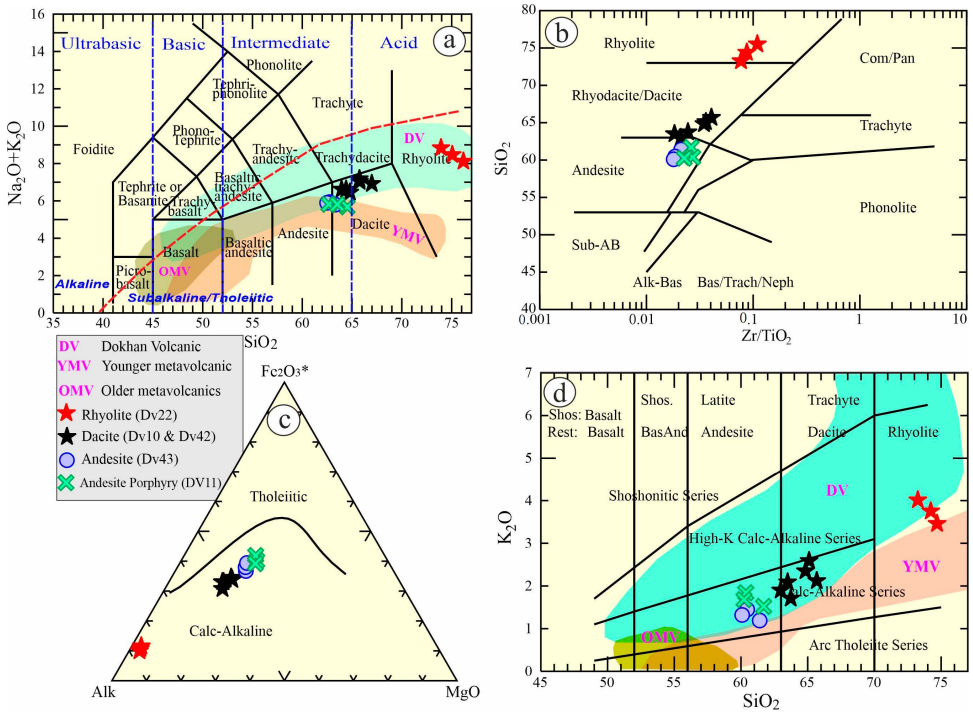

Figure 6. *Cont.*

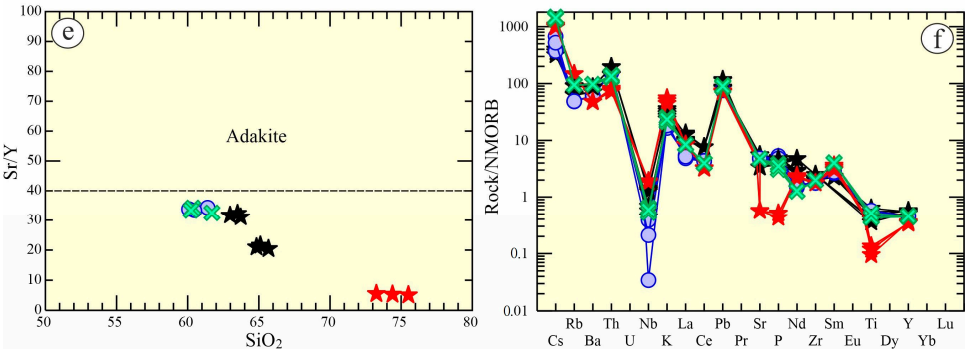

Figure 6. (**a**) TAS binary diagram [85]; (**b**) Zr/TiO_2-SiO_2 diagram [79]; (**c**) AFM ternary diagram [80]; (**d**) K_2O-SiO_2 diagram [81]; (**e**) SiO_2-Sr/Y [82], and (**f**) N-MORB diagram for the examined rocks [90]. Fields for comparison are YMV and OMV [91]. The DV field adapted from [2,7,9,92].

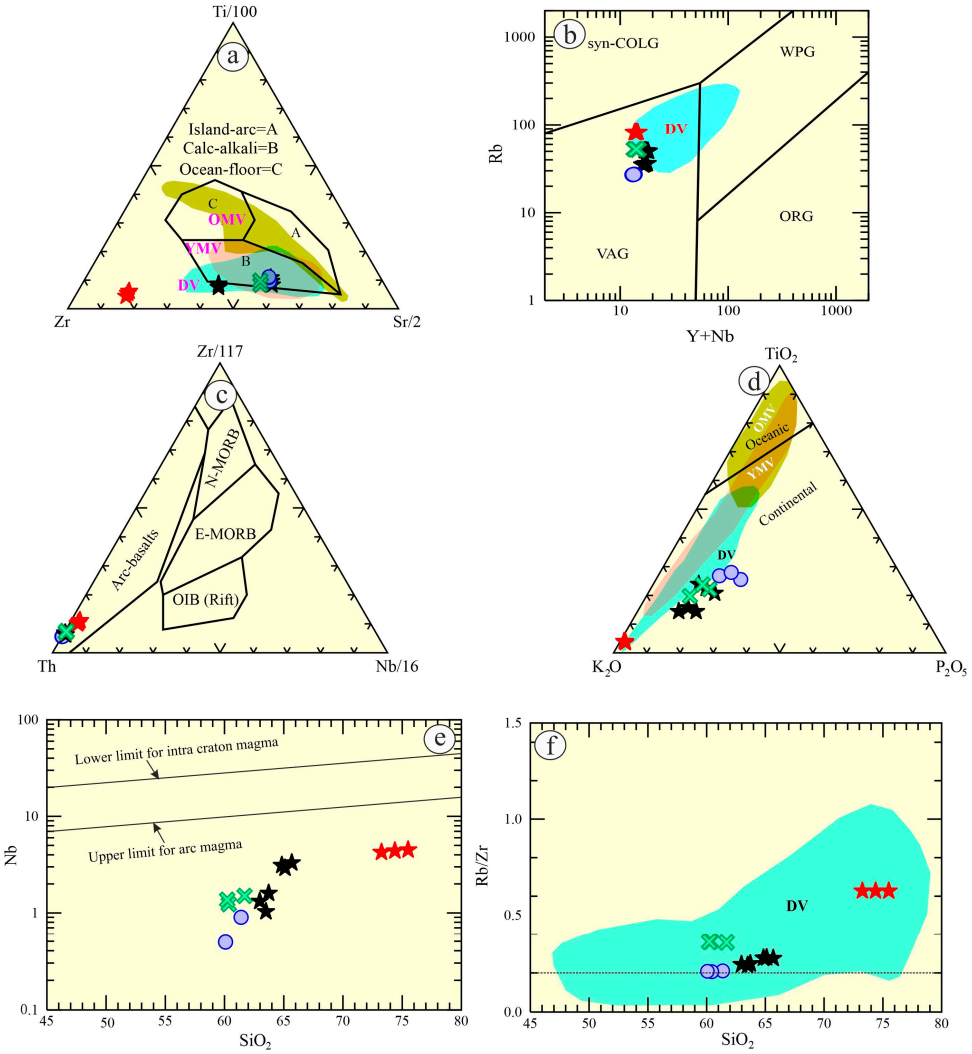

Figure 7. (**a**) Sr/2-Ti/100-Zr [85]; (**b**) Nb+Y-Rb of [86]; (**c**) Th-Hf-Nb diagram [87]; (**d**) P_2O_5-K_2O-TiO_2 of [88]; (**e**) SiO_2-Nb-SiO_2 [89]; and (**f**) Rb/Zr-SiO_2 diagram [2]. Symbol's explanation are consistent with Figure 6.

5.2.3. Petrogenesis

Certain limitations on the nature of the magma sources during the Neoproterozoic in the Northeastern Desert of Egypt can be obtained from their petrochemical data. The examined DV samples demonstrate clear negative anomalies for Ti and Nb, and they are

medium- to high-K and richer in LILE in comparison to HFSE. In reality, these characteristics are indicative of a calc-alkaline orogenic setting [93]. On the other hand, during the post-collisional phase, these characteristics might be the result of magmas originating from the mantle that has undergone prior metasomatism during the early orogenic stage [9,10]. Many authors ascribed the post-collisional intrusive and their equivalent extrusive rocks to the melting with different partial degrees of mafic source [9,27,36]. The lack or infrequent appearance of mafic units in the current volcanic eruptions indicates that the primary magma is not mantle-derived. This is supported by the Mg# of the current DV rocks, which range from 17.86 in rhyolite to 33.57 in andesite porphyry. Additionally, the examined DV rocks have Y/Nb ratios above 1.2, suggesting a crustal source [94].

We suggest that the partial melting of the lower crust can produce andesitic magma, which ascends to higher crustal levels and forms lava of calc-alkaline. A portion of this lava may split, settle at shallow crustal depths, and undergo differentiation to create the DV rocks [10,95]. The role of fractionation is interpreted by their variation from andesite passing through dacite to rhyolite, which is indicated by gradual negative distribution groups between silica and TiO_2, Fe_2O_3, CaO, MgO, Co, and Cu from andesite to rhyolitic lava (Figure 8). Further constraints include depletion in Ti and Nb, Sr, and P in rhyolite on the N-MORB/rock diagram, favoring the process of fractionation. On the other hand, for detecting the role of contamination/mingling processes, some ratios of trace elements are widely used, like Y/Nb, Rb/Zr, and Ba/Nb. There is no discernible change in these ratios during fractionation [96]. The Rb/Zr values in the DV samples are widely varied (0.2–0.63), pointing to crustal contamination certainly in the rhyolitic rocks (Figure 7f). Moreover, the wide variations in Y/Nb and Ba/Nb suggest the significant role of contamination [96].

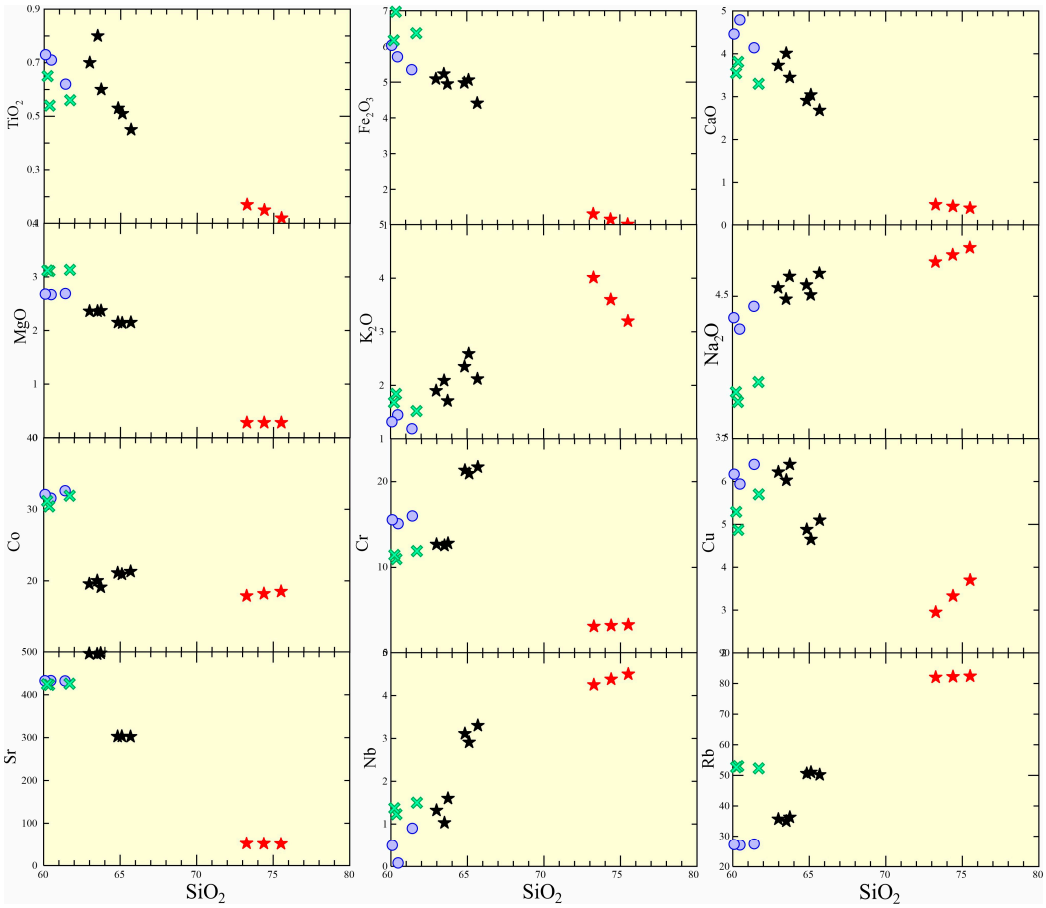

Figure 8. Binary (Harker) variation diagrams between SiO_2 and some major and trace elements. It is noticeable that there is a systematic, gradual distribution between different types of Dokhan volcanics. Symbol's explanation are consistent with Figure 6.

5.3. Decorative Applications of Dokhan Volcanics

The utilization of natural stones, such as Dokhan volcanics, as decorative dimension stones in outdoor and indoor installations involves performing their physical and mechanical properties compared with the international standard specifications. Water absorption, bulk-specific gravity (density), porosity, compressive strength, and abrasion resistance are the main properties that evaluate the performance of natural stones and their suitability for decorative purposes (Table 2).

Table 2. Provides outcomes of mechanical and physical attributes of the studied specimens with minimum, maximum, and average values.

Measured Parameters	Statistical Parameters	Studied Rock Specimens					Reference Standard, ASTM C615 [97]
		DV 10	DV 11	DV 42	DV 43	DV 22	
Water absorption, %	Max.	0.07	0.09	0.08	0.06	0.62	0.4% max.
	Min.	0.05	0.07	0.06	0.05	0.53	
	Av.	0.06	0.08	0.06	0.06	0.58	
Apparent porosity, %	Max.	0.18	0.24	0.21	0.18	1.62	N/A
	Min.	0.14	0.21	0.16	0.14	1.37	
	Av.	0.16	0.23	0.18	0.16	1.52	
Dry bulk density, kg/m^3	Max.	2728.08	2772.23	2756.81	2771.11	2606.82	2560 kg/m^3 min.
	Min.	2723.81	2760.56	2747.59	2757.32	2600.03	
	Av.	2726.54	2766.29	2752.77	2764.86	2603.07	
Wet bulk density, kg/m^3	Max.	2729.58	2772.66	2758.41	2772.50	2620.52	N/A
	Min.	2725.64	2762.88	2749.66	2759.07	2615.69	
	Av.	2728.12	2768.56	2754.54	2766.42	2618.27	
Compressive strength, kg/cm^2 (MPa)	Max.	1634.38 (160.28)	1625.54 (159.41)	1234.58 (121.07)	1360.92 (133.46)	1515.05 (148.58)	131 MPa min.
	Min.	690.59 (67.72)	802.83 (78.73)	1141.22 (111.92)	817.89 (80.21)	798.25 (78.28)	
	Av.	1130.21 (110.84)	1240.69 (121.67)	1189.10 (116.61)	1196.98 (117.38)	1219.30 (119.57)	
Abrasion resistance, Ha (Groove width)	Max.	58.63 (15.04)	34.14 (18.28)	43.16 (16.81)	33.73 (18.36)	37.82 (17.62)	25 Ha min.
	Min.	32.07 (18.69)	26.52 (19.99)	32.08 (18.69)	21.01 (21.69)	21.79 (21.41)	
	Av.	42.67 (17.15)	30.25 (19.13)	36.43 (17.93)	29.49 (19.41)	28.88 (19.63)	

Looking at the results of the physical measurements, it is clear that there is a convergence in the values of water absorption, apparent porosity, and bulk density for the rock units DV10, DV11, DV42, and DV43. For water absorption test results, as shown in Figure 9a, the average values were found to be 0.06%, 0.08%, 0.06%, and 0.06%, respectively, that met the requirements of the granite dimension stone (max. 0.4%) according to [97].

Compared to the literature related to dimension stones, the rock types DV10, DV11, DV42, and DV43 revealed a lower water absorption and, consequently, porosity than reported by Alzahrani et al. [34] (0.14–0.31%) and Siegesmund et al. [40] (0.3–3.37%) for granitic stones.

For bulk density test results, as shown in Figure 9b, the average values were reported as 2726.54 kg/m^3, 2766.29 kg/m^3, 2752.77 kg/m^3, and 2764.86 kg/m^3, respectively, which also met the requirements of the granite dimension stones (min. 2560 kg/m^3). Compared to the literature, the rock types DV10, DV11, DV42, and DV43 also achieved higher bulk density than all studied granitic stones, such as 2.58–2.68 g/cm^3 [98] and 2.55–2.84 g/cm^3 [20,99]. As for the rock sample DV22, it exhibited different physical results from the previous rock types, with a high-water absorption value (av. 0.58%) and low bulk density value (av. 2603.07 kg/m^3).

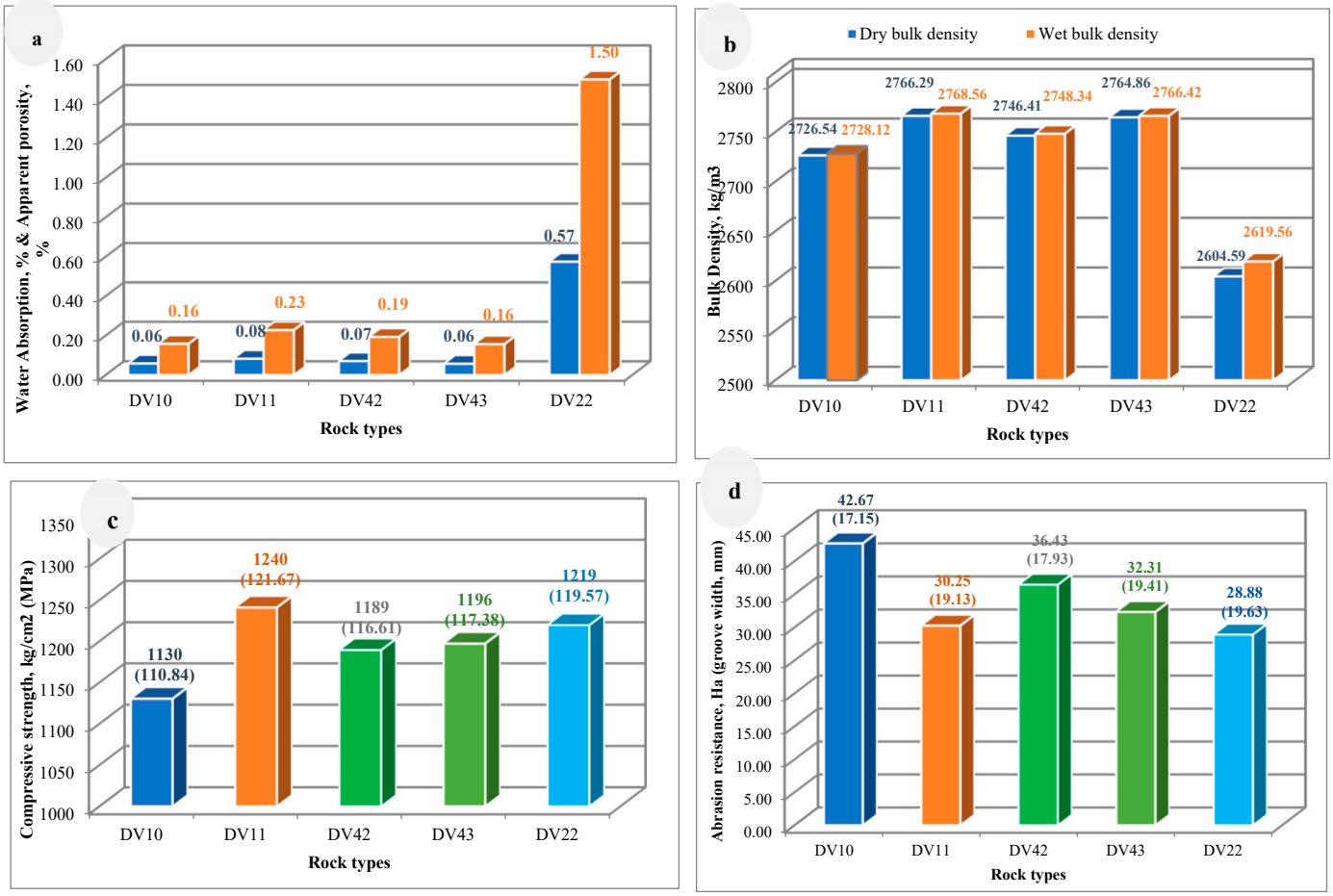

Figure 9. (**a**) Average water absorption and apparent porosity of different DV rock units; (**b**) Average dry and wet bulk density of different DV rock units; (**c**) Average compressive strength of different DV rock units; and (**d**) Average abrasion resistance of different DV rock units.

Regarding the mechanical measurements, the results displayed a similarity in the values of compressive strength and abrasion resistance between the studied rock samples. As shown in (Figure 9c), the average values of the compressive strength test were calculated in kg/cm^2 (MPa) for DV10, DV11, DV42, DV43, and DV22 as 1130 (110.84), 1240 (121.67), 1189 (116.91), 1196 (117.38), and 1219 (119.57), respectively, although the values of the compressive strength test did not achieve the minimum limit of the granite dimension stone specification (1335 kg/cm^2 or 131 MPa); however, it may be used for other applications such as interior or exterior cladding and monuments provided that other relevant characteristics shall be evaluated such as durability, permanent volume change, thermal expansion, and modulus of elasticity [97]. Regarding the abrasion resistance test, Figure 9d illustrates the average results of the studied rock samples. The average results were calculated in Ha or (mm) as follows: 42.67 (17.15); 30.25 (19.13); 36.43 (17.93); 29.49 (19.41); and 28.88 (19.63) for DV10, DV11, DV42, DV43, and DV22; respectively.

Comparing the test results considering dimension stones' typical specifications, it is observed that all the studied rock units exceeded the required minimum limit of abrasion resistance (25 Ha). By correlating the physical characteristics of the samples under study, we can observe a strong positive relationship between water absorption and apparent porosity with a correlation coefficient (R^2 = 1), as illustrated in Figure 10a. Therefore, there is a strong negative relationship between porosity and dry and wet bulk density, as shown in Figure 10b, with correlation coefficients (R^2 = 0.92 and 0.91), respectively.

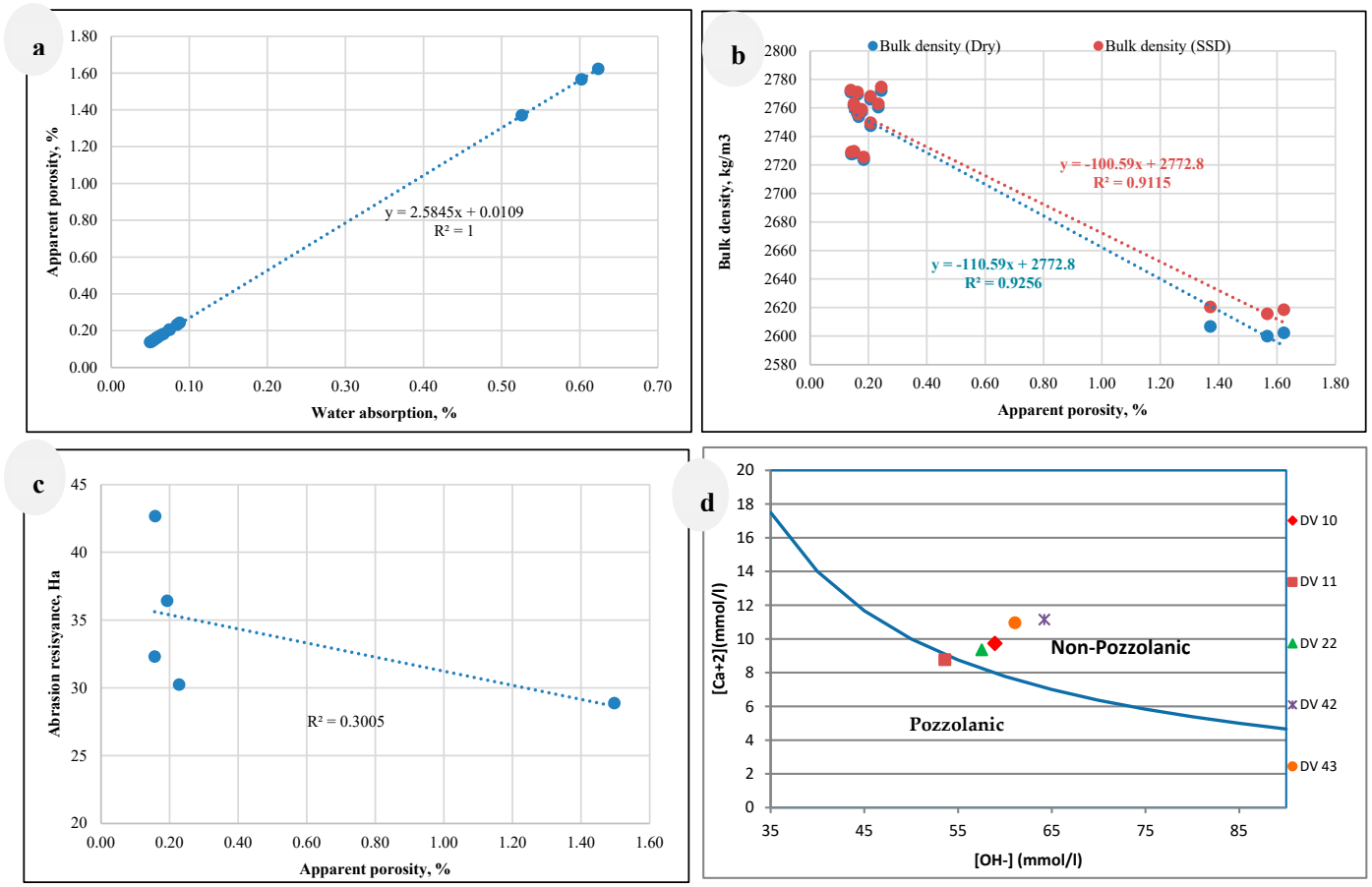

Figure 10. Relationships of the studied DV rock units: (**a**) water absorption and apparent porosity; (**b**) dry and wet bulk densities and apparent porosity; (**c**) abrasion resistance and apparent porosity; and (**d**) pozzolanic assessment of different DV rock units.

As any rock type consists of porosity in the form of cracks or veins resulting from either mechanical deformation or chemical decomposition by weathering, these kinds of porosity could reduce the durability of the material by weakening the cohesiveness between its grains [30,36,54]. Therefore, according to the previous relationship between water absorption, porosity, and density, it is suggested from a practical view that any rock type of low density due to its high porosity content can be installed indoors, avoiding the deterioration effect resulting from high water absorption, as well as low abrasion resistance. Figure 10c shows a negative correlation coefficient between the rocks' apparent porosities and their abrasion resistance ratings (Ha) by (R^2 = 0.3).

5.4. Pozzolanic Activity of Dokhan Volcanics

In the present study, two parameters are used to determine the degree of pozzolanic activity of the studied volcanic rocks: the first is determining their chemical composition, particularly the percentages of SiO_2, Al_2O_3, and Fe_2O_3 oxides. Comparing the results of chemical composition (Table 1) with the standard specification [76], it was found that the sum of (SiO_2+ Al_2O_3+ Fe_2O_3) of the studied rock samples that are calculated at 85.99%, 82.84%, 85.11%, 82.90%, and 89.81% for DV10, DV11, DV42, DV43, and DV22, respectively, achieved the minimum requirement (70%). The second parameter measures their pozzolanicity based on Frattini's test to determine whether the values lie in the pozzolanic or non-pozzolanic areas. Figure 10d shows that the volcanic rock sample (DV22) is plotted within the pozzolanic area, while the other samples are plotted within the non-pozzolanic area.

It was found that the sample (DV22) exhibited superior pozzolanic behavior due to several factors. Despite all samples exceeding ASTM C618 [76] limiting of 70% oxide summation, the sample's (DV22) notably higher value of 89.81% facilitated a more pronounced reaction with calcium hydroxide. Additionally, according to Table 2, the sample (DV22) showed the highest water absorption and porosity values, with about tenfold the other samples values. This suggests the formation of pores within the rock, possibly resulting from sudden temperature fluctuations in the magma that promoted the release of soluble gases. Coupled with its high silica content, this evidence indicates a substantial amount of amorphous glass phase, combined with a porous morphology, contributing to DV22's enhanced pozzolanic properties.

Further research is necessary to determine the optimal percentage of sample DV22 to be added to OPC to achieve the best physical and mechanical properties. It is important to note that each ton of produced OPC generates approximately 0.9 tons of carbon dioxide [100]. Therefore, incorporating 10% of sample DV22 into OPC is estimated to reduce carbon dioxide emissions by roughly 90 kg.

6. Conclusions

The current work provides petrographical, petrological, physico-mechanical, and pozzolanic assessments of some lava from the type locality of the DV in order to deduce their setting and petrogenesis, as well as their favorability as a decorative stone and perspective as a natural pozzolanic in building materials. The DV have a distinct, dense series of stratified, rhyolitic to andesitic lava interspersed with a few pyroclastic layers that suggest a series of explosions. Chemically, they are medium-K and high-K calc-alkaline with an agpaitic index of less than 0.84. They are normal arc rocks rather than adakites due to low Y (9.45–16) and Sr/Y (5.07–34.3) contents. In comparison to N-MORB, all the DV samples display enrichment in Ba, Rb, Pb, and K, but much depletion in Ti and Nb, besides Sr and P in rhyolite (as a result of fractionation of iron oxides, feldspar, and apatite), supporting their subduction-related rather than post-collisional and followed by fractionation and crustal contamination. For decorative purposes, the physico-mechanical measurements of the studied Dokhan volcanic rocks revealed that their water absorption, bulk density, and resistance to abrasion ranged from 0.06 to 0.57%, 2605.59 to 2766.29 kg/m^3, and 28.88 to 42.67 Ha, respectively, that fulfilled the requirements of the standard specifications. Concerning the compressive strength, the results revealed that even though the average values fell short of the minimal standards, they might still be suitable for light-duty applications like indoor use and exterior applications like cladding and façades. Based on the pozzolanic assessment of the studied rock types, the results revealed the possibility of using these natural stones as supplementary cementitious materials in the building sector. Furthermore, in the same sector and based on their hardness, compactness, and resistance to wear, the studied rock types can be crushed as aggregate materials of various sizes in mortar, concrete, and asphalt mixes. Finally, the authors recommend further experimental studies in the future, focusing on their effect on physico-mechanical and durability performance of mortar and concrete products.

Author Contributions: Conceptualization, E.S.R.L., M.A.R. and M.S.; data curation, E.S.R.L., M.A.R. and A.A.H.; funding acquisition I.V.S., H.A. and M.S.A.; investigation, E.S.R.L., M.A.R., M.S.A. and A.A.H.; methodology, M.S., M.A.R. and E.S.R.L.; project administration, M.S. and E.S.R.L.; software, E.S.R.L., M.A.R., A.A.H. and M.S.; supervision, E.S.R.L., M.A.R., M.S., H.A. and I.V.S.; validation, E.S.R.L., H.A., M.S. and M.S.A.; visualization, E.S.R.L., M.A.R., H.A., I.V.S. and M.S.; writing—original draft E.S.R.L., M.A.R., M.S. and A.A.H.; writing—review and editing, E.S.R.L., M.A.R., A.A.H. and M.S. All authors have read and agreed to the published version of the manuscript.

Funding: This research was funded by Researchers Supporting Project Number (RSP2024R455), King Saud University, Riyadh, Saudi Arabia.

Data Availability Statement: The linked authors can provide the data regarding this study upon request.

Acknowledgments: The authors would like to thank the "Marble and Granite Test Lab" unit (MGTL), the pioneer in the field dimension stones in Egypt at the National Research Centre (NRC), for measuring the mechanical and physical tests. Also, they appreciate the helpful of XRF Lab for chemical analysis measurements. This research was funded by Researchers Supporting Project Number (RSP2024R455), King Saud University, Riyadh, Saudi Arabi.

Conflicts of Interest: There are no conflicts of interest.

References

1. Sami, M.; Faisal, M.; Leybourne, M.; Sanislav, I.V.; Ahmed, M.S.; Lasheen, E.S.R. Unravelling the Genesis and Depositional Setting of Neoproterozoic Banded Iron Formation from Central Eastern Desert, Egypt. *Front. Earth Sci.* **2024**, *12*, 1359617. [CrossRef]
2. Moghazi, A.M. Geochemistry and Petrogenesis of a High-K Calc-Alkaline Dokhan Volcanic Suite, South Safaga Area, Egypt: The Role of Late Neoproterozoic Crustal Extension. *Precambrian Res.* **2003**, *125*, 161–178. [CrossRef]
3. Khaleal, F.M.; Lentz, D.R.; Kamar, M.S.; Saleh, G.M.; Lasheen, E.S.R. Critical Raw Material Resources in Nugrus-Sikait Area, South Eastern Desert, Egypt: Geological and Geochemical Aspects. *J. Afr. Earth Sci.* **2023**, *197*, 104782. [CrossRef]
4. Stern, R.J. Neoproterozoic Formation and Evolution of Eastern Desert Continental Crust—The Importance of the Infrastructure-Superstructure Transition. *J. Afr. Earth Sci.* **2018**, *146*, 15–27. [CrossRef]
5. Khaleal, F.M.; Lentz, D.R.; Kamh, S.Z.; Saleh, G.M.; Abdalla, F.; Lasheen, E.S.R. Remote Sensing Analysis and Geodynamic Setting of Magmatic Spessartine-Almandine-Bearing Leucogranites, Um Addebaa Area, Southeastern Desert, Egypt: Bulk Rock and Mineral Chemistry. *Phys. Chem. Earth Parts ABC* **2024**, *136*, 103749. [CrossRef]
6. Saleh, G.M.; Kamh, S.Z.; Abdalla, F.; Kilias, A.; Lasheen, E.S.R. A New Occurrence of Rift-Related Damtjernite (Ultramafic) Lamprophyre, Gebel Anweiyib Area, Arabian Nubian Shield: Insights from Bulk Rock Geochemistry and Remote Sensing Data Analysis. *Phys. Chem. Earth Parts ABC* **2024**, *133*, 103530. [CrossRef]
7. Abdel-Rahman, A.-F.M. Pan-African Volcanism: Petrology and Geochemistry of the Dokhan Volcanic Suite in the Northern Nubian Shield. *Geol. Mag.* **1996**, *133*, 17–31. [CrossRef]
8. Abuamarah, B.A.; Azer, M.K.; Asimow, P.D.; Shi, Q. Post-Collisional Volcanism with Adakitic Signatures in the Arabian-Nubian Shield: A Case Study of Calc-Alkaline Dokhan Volcanics in the Eastern Desert of Egypt. *Lithos* **2021**, *388–389*, 106051. [CrossRef]
9. Eliwa, H.A.; Kimura, J.-I.; Itaya, T. Late Neoproterozoic Dokhan Volcanics, North Eastern Desert, Egypt: Geochemistry and Petrogenesis. *Precambrian Res.* **2006**, *151*, 31–52. [CrossRef]
10. Obeid, M.A.; Azer, M.K. Pan-African Adakitic Rocks of the North Arabian–Nubian Shield: Petrological and Geochemical Constraints on the Evolution of the Dokhan Volcanics in the North Eastern Desert of Egypt. *Int. J. Earth Sci.* **2015**, *104*, 541–563. [CrossRef]
11. Seddiek, S.H.; El Afandy, A.H.; El Kaliouby, B.A.; Eliwa, H.A.; Khamis, H.A. Petrological and Geochemical Investigations on Dokhan Volcanics at Wadi Um Sidra-Wadi Um Asmer Area, North Eastern Desert, Egypt. *Egypt J. Geol.* **2020**, *64*, 237–254.
12. Wilde, S.A.; Youssef, K. Significance of SHRIMP U-Pb Dating of the Imperial Porphyry and Associated Dokhan Volcanics, Gebel Dokhan, North Eastern Desert, Egypt. *J. Afr. Earth Sci.* **2000**, *31*, 403–413. [CrossRef]
13. Hassan, M.A.; Hashad, A.H. Precambrian Egypt. In *Geology of Egypt*; Said, R., Ed.; Balkema: Rotterdam, The Netherlands, 1990.
14. Fritz, H.; Wallbrecher, E.; Khudeir, A.A.; Abu El Ela, F.; Dallmeyer, D.R. Formation of Neoproterozoic Metamorphic Complex during Oblique Convergence (Eastern Desert, Egypt). *J. Afr. Earth Sci.* **1996**, *23*, 311–329. [CrossRef]
15. Sami, M.; Azer, M.; Abdel-Karim, A.A. Postcollisional Ferani volcanics from north Arabian–Nubian Shield (south Sinai, Egypt): Petrogenesis and implication for Ediacaran (607–593 Ma) geodynamic evolution. *J. Geo.* **2022**, *130*, 475–498. [CrossRef]
16. Mohamed, F.H.; Moghazi, A.M.; Hassanen, M.A. Geochemistry, Petrogenesis and Tectonic Setting of Late Neoproterozoic Dokhan-Type Volcanic Rocks in the Fatira Area, Eastern Egypt. *Int. J. Earth Sci.* **2000**, *88*, 764–777. [CrossRef]
17. Wahab, G.M.A.; Gouda, M.; Ibrahim, G. Study of Physical and Mechanical Properties for Some of Eastern Desert Dimension Marble and Granite Utilized in Building Decoration. *Ain Shams Eng. J.* **2019**, *10*, 907–915. [CrossRef]
18. *ASTM C119*; Standard Terminology Relating to Dimension Stone American Society for Testing and Materials. ASTM International: West Conshohocken, PA, USA, 2014.
19. Careddu, N. Dimension Stones in the Circular Economy World. *Resour. Policy* **2019**, *60*, 243–245. [CrossRef]
20. Freire-Lista, D.M. The Forerunners on Heritage Stones Investigation: Historical Synthesis and Evolution. *Heritage* **2021**, *4*, 1228–1268. [CrossRef]
21. Mosch, S.; Siegesmund, S. Petrophysical and Technical Properties of Dimensional Stones: A Statistical Approach. *Zeitschrift der Deutschen Gesellschaft für Geowissenschaften* **2007**, *158*, 821–868. [CrossRef]
22. Sitzia, F.; Lisci, C.; Mirão, J. Accelerate Ageing on Building Stone Materials by Simulating Daily, Seasonal Thermo-Hygrometric Conditions and Solar Radiation of Csa Mediterranean Climate. *Constr. Build. Mater.* **2021**, *266*, 121009. [CrossRef]
23. Vigroux, M.; Eslami, J.; Beaucour, A.-L.; Bourgès, A.; Noumowé, A. High Temperature Behaviour of Various Natural Building Stones. *Constr. Build. Mater.* **2021**, *272*, 121629. [CrossRef]
24. Marble Institute of America Geology of Stone. 2011. Available online: www.Marble-Institute.Com (accessed on 1 January 2024).
25. Ciccu, R.; Cosentino, R.; Montani, C.; El Kotb, A.; Hamdy, H. *Strategic Study on the Egyptian Marble and Granite Sector*; Industrial Modernization Centre: Cairo, Egypt, 2005.

26. Gomes, V.R.; Babisk, M.P.; Vieira, C.M.F.; Sampaio, J.A.; Vidal, F.W.H.; Gadioli, M.C.B. Ornamental Stone Wastes as an Alternate Raw Material for Soda-Lime Glass Manufacturing. *Mater. Lett.* **2020**, *269*, 127579. [CrossRef]
27. Lasheen, E.S.R.; Elyaseer, M.H.; Mohamed, W.H.; Azer, M.K.; Rashwan, M.A.; Thabet, I.A. Economic Feasibility of Gabal Um Takha Leucogranitic Intrusion, South Sinai, Egypt: Integrated Remote Sensing, Geochemical, Aeromagnetic, and Geotechnical Approach. *Phys. Chem. Earth Parts A/B/C* **2024**, *133*, 103531. [CrossRef]
28. Rashwan, M.A.; Lasheen, E.S.R.; Azer, M.K. Thermal and Physico-Mechanical Evaluation of Some Magmatic Rocks at Homrit Waggat Area, Eastern Desert, Egypt: Petrography and Geochemistry. *Bull. Eng. Geol. Environ.* **2023**, *82*, 199. [CrossRef]
29. Mashaly, A.O.; El-Kaliouby, B.A.; Shalaby, B.N.; El-Gohary, A.M.; Rashwan, M.A. Effects of Marble Sludge Incorporation on the Properties of Cement Composites and Concrete Paving Blocks. *J. Clean. Prod.* **2016**, *112*, 731–741. [CrossRef]
30. Rashwan, M.A.; Lasheen, E.S.R.; Abdelwahab, W.; Azer, M.K.; Zakaly, H.M.H.; Alarifi, S.S.; Ene, A.; Thabet, I.A. Physico-Mechanical Properties and Shielding Efficiency in Relation to Mineralogical and Geochemical Compositions of Um Had Granitoid, Central Eastern Desert, Egypt. *Front. Earth Sci.* **2023**, *11*, 1228489. [CrossRef]
31. Ericsson, M. XXIX World Marble and Stones Report 2018 by Carlo Montani: Aldus Casa Di Edizioni, Carrara Italy 2018 E-Mail: Aldus.Danielecanal@alice.It. *Miner. Econ.* **2019**, *32*, 255–256. [CrossRef]
32. Rana, A.; Kalla, P.; Verma, H.K.; Mohnot, J.K. Recycling of Dimensional Stone Waste in Concrete: A Review. *J. Clean. Prod.* **2016**, *135*, 312–331. [CrossRef]
33. Singh Chouhan, H.; Kalla, P.; Nagar, R.; Kumar Gautam, P. Influence of Dimensional Stone Waste on Mechanical and Durability Properties of Mortar: A Review. *Constr. Build. Mater.* **2019**, *227*, 116662. [CrossRef]
34. Alzahrani, A.M.; Lasheen, E.S.R.; Rashwan, M.A. Relationship of Mineralogical Composition to Thermal Expansion, Spectral Reflectance, and Physico-Mechanical Aspects of Commercial Ornamental Granitic Rocks. *Materials* **2022**, *15*, 2041. [CrossRef]
35. Rashwan, M.A.; Abd El-Shakour, Z.A. Low-Cost, Highly-Performance Fired Clay Bodies Incorporating Natural Stone Sludge: Microstructure and Engineering Properties. *Clean. Waste Syst.* **2022**, *3*, 100041. [CrossRef]
36. Lasheen, E.S.R.; Rashwan, M.A.; Azer, M.K. Effect of Mineralogical Variations on Physico-Mechanical and Thermal Properties of Granitic Rocks. *Sci. Rep.* **2023**, *13*, 10320. [CrossRef] [PubMed]
37. Freire-Lista, D.M.; Gonçalves, G.V.; Vazquez, P. Weathering Detection of Granite from Three Asynchronous Historical Quarries of Sabrosa Municipally (North Portugal). *J. Cult. Herit.* **2022**, *58*, 199–208. [CrossRef]
38. Heuze, F.E. High-Temperature Mechanical, Physical and Thermal Properties of Granitic Rocks—A Review. *Int. J. Rock Mech. Min. Sci. Geomech. Abstr.* **1983**, *20*, 3–10. [CrossRef]
39. Huotari, T.K.; Kukkonen, I. *Thermal Expansion Properties of Rocks: Literature Survey and Fstimation of Thermal Expansion Coefficient for Olkiluoto Mica Gneiss*; Geological Survey of Finland: Espoo, Finland, 2004.
40. Siegesmund, S.; Sousa, L.; Knell, C. Thermal Expansion of Granitoids. *Environ. Earth Sci.* **2018**, *77*, 41. [CrossRef]
41. Agasnalli, C.; Hema, H.C.; Lakkundi, T.; Chandrappa, K.D. Integrated Assessment of Granite and Basalt Rocks as Building Materials. *Mater. Today Proc.* **2022**, *62*, 5388–5391. [CrossRef]
42. Sivanandhini, K.; Subasree, S.; Preethika, R.; Meenakshi, M. Experimental Study on Using Basalt as a Construction Material. *Int. J. Civ. Eng.* **2019**, *6*, 11–12. [CrossRef]
43. Dobiszewska, M.; Schindler, A.K.; Pichór, W. Mechanical Properties and Interfacial Transition Zone Microstructure of Concrete with Waste Basalt Powder Addition. *Constr. Build. Mater.* **2018**, *177*, 222–229. [CrossRef]
44. Ingrao, C.; Lo Giudice, A.; Tricase, C.; Mbohwa, C.; Rana, R. The Use of Basalt Aggregates in the Production of Concrete for the Prefabrication Industry: Environmental Impact Assessment, Interpretation and Improvement. *J. Clean. Prod.* **2014**, *75*, 195–204. [CrossRef]
45. Kılıç, A.; Atiş, C.D.; Teymen, A.; Karahan, O.; Özcan, F.; Bilim, C.; Özdemir, M. The Influence of Aggregate Type on the Strength and Abrasion Resistance of High Strength Concrete. *Cem. Concr. Compos.* **2008**, *30*, 290–296. [CrossRef]
46. Korkanç, M.; Tuğrul, A. Evaluation of Selected Basalts from Niğde, Turkey, as Source of Concrete Aggregate. *Eng. Geol.* **2004**, *75*, 291–307. [CrossRef]
47. Li, P.P.; Yu, Q.L.; Brouwers, H.J.H. Effect of Coarse Basalt Aggregates on the Properties of Ultra-High Performance Concrete (UHPC). *Constr. Build. Mater.* **2018**, *170*, 649–659. [CrossRef]
48. Piasta, W.; Góra, J.; Turkiewicz, T. Properties and Durability of Coarse Igneous Rock Aggregates and Concretes. *Constr. Build. Mater.* **2016**, *126*, 119–129. [CrossRef]
49. Davraz, M.; Ceylan, H.; Topçu, İ.B.; Uygunoğlu, T. Pozzolanic Effect of Andesite Waste Powder on Mechanical Properties of High Strength Concrete. *Constr. Build. Mater.* **2018**, *165*, 494–503. [CrossRef]
50. Ghorbani, S.; Taji, I.; De Brito, J.; Negahban, M.; Ghorbani, S.; Tavakkolizadeh, M.; Davoodi, A. Mechanical and Durability Behaviour of Concrete with Granite Waste Dust as Partial Cement Replacement under Adverse Exposure Conditions. *Constr. Build. Mater.* **2019**, *194*, 143–152. [CrossRef]
51. Labbaci, Y.; Abdelaziz, Y.; Mekkaoui, A.; Alouani, A.; Labbaci, B. The Use of the Volcanic Powders as Supplementary Cementitious Materials for Environmental-Friendly Durable Concrete. *Constr. Build. Mater.* **2017**, *133*, 468–481. [CrossRef]
52. Laibao, L.; Yunsheng, Z.; Wenhua, Z.; Zhiyong, L.; Lihua, Z. Investigating the Influence of Basalt as Mineral Admixture on Hydration and Microstructure Formation Mechanism of Cement. *Constr. Build. Mater.* **2013**, *48*, 434–440. [CrossRef]
53. Mashaly, A.O.; Shalaby, B.N.; Rashwan, M.A. Performance of Mortar and Concrete Incorporating Granite Sludge as Cement Replacement. *Constr. Build. Mater.* **2018**, *169*, 800–818. [CrossRef]

54. Rashwan, M.A.; Lasheen, E.S.R.; Hegazy, A.A. Tracking the Pozzolanic Activity of Mafic Rock Powder on Durability Performance of Cement Pastes under Adverse Conditions: Physico-Mechanical, Mineralogy, Microstructure, and Heat of Hydration. *J. Build. Eng.* **2023**, *71*, 106485. [CrossRef]
55. Rashwan, M.A.; Al-Basiony, T.M.; Mashaly, A.O.; Khalil, M.M. Behaviour of Fresh and Hardened Concrete Incorporating Marble and Granite Sludge as Cement Replacement. *J. Build. Eng.* **2020**, *32*, 101697. [CrossRef]
56. Rashwan, M.A.; Lasheen, E.S.R.; Shalaby, B.N. Incorporation of Metagabbro as Cement Replacement in Cement-Based Materials: A Role of Mafic Minerals on the Physico-Mechanical and Durability Properties. *Constr. Build. Mater.* **2019**, *210*, 256–268. [CrossRef]
57. Saraya, M.E.-S.I. Study Physico-Chemical Properties of Blended Cements Containing Fixed Amount of Silica Fume, Blast Furnace Slag, Basalt and Limestone, a Comparative Study. *Constr. Build. Mater.* **2014**, *72*, 104–112. [CrossRef]
58. Singh, S.; Anshumantiwari; Nagar, R.; Agrawal, V. Feasibility as a Potential Substitute for Natural Sand: A Comparative Study between Granite Cutting Waste and Marble Slurry. *Procedia Environ. Sci.* **2016**, *35*, 571–582. [CrossRef]
59. Hegazy, A.; Khalil, A.; El-Alfi, E.; El-Shahat, M. Durability of Supersulphated Cement Pastes Activated with Portland Cement in Magnesium Chloride Solution. *Egypt J. Chem.* **2019**, *62*, 1145–1155. [CrossRef]
60. *ASTM C125*; Standard Terminology Relating to Concrete and Concrete Aggregates American Society for Testing and Materials. ASTM International: West Conshohocken, PA, USA, 2015.
61. Massazza, F. Pozzolana and Pozzolanic Cements. In *Lea's Chemistry of Cement and Concrete*; Hewlett, P., Ed.; Elsevier Science: Amsterdam, The Netherlands, 2004.
62. Scherer, C.; Felippi De Lima, L.; Eunice Zorzi, J. Effect of Partial Replacement of Cement by Fine Powders on the Corrosion Resistance of Concrete. *Constr. Build. Mater.* **2023**, *401*, 132982. [CrossRef]
63. Yang, R.; Yu, R.; Shui, Z.; Gao, X.; Han, J.; Lin, G.; Qian, D.; Liu, Z.; He, Y. Environmental and Economical Friendly Ultra-High Performance-Concrete Incorporating Appropriate Quarry-Stone Powders. *J. Clean. Prod.* **2020**, *260*, 121112. [CrossRef]
64. Scheinherrová, L.; Keppert, M.; Černý, R. Chemical Aspects of the Application of Basalt in Cement Composites. *Constr. Build. Mater.* **2022**, *350*, 128873. [CrossRef]
65. Türk, E.; Karataş, M.; Dener, M. Rheological, Mechanical and Durability Properties of Self-Compacting Mortars Containing Basalt Powder and Silica Fume. *Constr. Build. Mater.* **2022**, *356*, 129229. [CrossRef]
66. Baki, V.A.; Nayir, S.; Erdogdu, S.; Ustabas, I. Pozzolanic Properties of Trachyte and Rhyolite and Their Effects on Alkali-Silica Reaction. *Adv. Concr. Constr.* **2021**, *11*, 299–306. [CrossRef]
67. Çullu, M.; Bolat, H.; Vural, A.; Tuncer, E. Investigation of Pozzolanic Activity of Volcanic Rocks from the Northeast of the Black Sea. *Sci. Eng. Compos. Mater.* **2016**, *23*, 315–323. [CrossRef]
68. *ASTM E1621*; Standard Guide for Elemental Analysis by Wavelength Dispersive X-Ray Fluorescence Spectrometry. American Society for Testing and Materials: West Conshohocken, PA, USA, 2013.
69. *ASTM D7348*; Standard Test Methods for Loss on Ignition (LOI) of Solid Combustion Residues. American Society for Testing and Materials: West Conshohocken, PA, USA, 2013.
70. *ASTM C97/C97M*; Standard Test Method for Absorption and Bulk Specific Gravity of Dimension Stone. American Society for Testing and Materials: West Conshohocken, PA, USA, 2015.
71. *EN 1936*; Natural Stone Test Methods—Determination of Real Density and Apparent Density, and of Total and Open Porosity. European Committee for Standardization (CEN): Brussels, Belgium, 1999.
72. *ASTM C170/C170M*; Standard Test Method for Compressive Strength of Dimension Stone. American Society for Testing and Materials: West Conshohocken, PA, USA, 2015.
73. *ASTM C241/C241M*; Standard Test Method for Abrasion Resistance of Stone Subjected to Foot Traffic. American Society for Testing and Materials: West Conshohocken, PA, USA, 2015.
74. *EN 14157*; Natural Stone Test Methods—Determination of the Abrasion Resistance. European Committee for Standardization: Brussels, Belgium, 2017.
75. *BS EN 196-5*; Methods of Testing Cement—Part 5: Pozzolanicity Test for Pozzolanic Cement. European Committee for Standardization: Brussels, Belgium, 2011.
76. *ASTM C618*; Standard Specification for Coal Fly Ash and Raw or Calcined Natural Pozzolan for Use in Concrete. American Society for Testing and Materials: West Conshohocken, PA, USA, 2003.
77. *ASTM C311/C311M*; Standard Test Methods for Sampling and Testing Fly Ash or Natural Pozzolans for Use in Portland-Cement Concrete. American Society for Testing and Materials: West Conshohocken, PA, USA, 2013.
78. Le Bas, M.J.L.; Maitre, R.W.L.; Streckeisen, A.; Zanettin, B.; IUGS Subcommission on the Systematics of Igneous Rocks. A Chemical Classification of Volcanic Rocks Based on the Total Alkali-Silica Diagram. *J. Petrol.* **1986**, *27*, 745–750. [CrossRef]
79. Winchester, J.A.; Floyd, P.A. Geochemical Discrimination of Different Magma Series and Their Differentiation Products Using Immobile Elements. *Chem. Geol.* **1977**, *20*, 325–343. [CrossRef]
80. Irvine, T.N.; Baragar, W.R.A. A Guide to the Chemical Classification of the Common Volcanic Rocks. *Can. J. Earth Sci.* **1971**, *8*, 523–548. [CrossRef]
81. Le Maitre, R.W. *A Classification of Igneous Rocks and Glossary of Terms*; Blackwell: Oxford, UK, 1989.
82. Defant, M.J.; Drummond, M.S. Derivation of Some Modern Arc Magmas by Melting of Young Subducted Lithosphere. *Nature* **1990**, *347*, 662–665. [CrossRef]

83. Woodhead, J.; Eggins, S.; Gamble, J. High Field Strength and Transition Element Systematics in Island Arc and Back-Arc Basin Basalts: Evidence for Multi-Phase Melt Extraction and a Depleted Mantle Wedge. *Earth Planet. Sci. Lett.* **1993**, *114*, 491–504. [CrossRef]
84. Stern, R.J.; Gottfried, D.; Hedge, C.E. Late Precambrian Rifting and Crustal Evolution in the Northeastern Desert of Egypt. *Geology* **1984**, *12*, 168. [CrossRef]
85. Pearce, J.A.; Cann, J.R. Tectonic Setting of Basic Volcanic Rocks Determined Using Trace Element Analyses. *Earth Planet. Sci. Lett.* **1973**, *19*, 290–300. [CrossRef]
86. Pearce, J.A.; Harris, N.B.W.; Tindle, A.G. Trace Element Discrimination Diagrams for the Tectonic Interpretation of Granitic Rocks. *J. Petrol.* **1984**, *25*, 956–983. [CrossRef]
87. Wood, D.A. The Application of a ThHfTa Diagram to Problems of Tectonomagmatic Classification and to Establishing the Nature of Crustal Contamination of Basaltic Lavas of the British Tertiary Volcanic Province. *Earth Planet. Sci. Lett.* **1980**, *50*, 11–30. [CrossRef]
88. Pearce, T.H.; Gorman, B.E.; Birkett, T.C. The TiO_2–K_2O–P_2O_5 Diagram: A Method of Discriminating between Oceanic and Non-Oceanic Basalts. *Earth Planet. Sci. Lett.* **1975**, *24*, 419–426. [CrossRef]
89. Pearce, J.A.; Gale, G.H. Identification of Ore-Deposition Environment from Trace-Element Geochemistry of Associated Igneous Host Rocks. *Geol. Soc. Lond. Spec. Publ.* **1977**, *7*, 14–24. [CrossRef]
90. Sun, S.-S.; McDonough, W.F. Chemical and Isotopic Systematics of Oceanic Basalts: Implications for Mantle Composition and Processes. *Geol. Soc. Lond. Spec. Publ.* **1989**, *42*, 313–345. [CrossRef]
91. Stern, R.J. Petrogenesis and Tectonic Setting of Late Precambrian Ensimatic Volcanic Rocks, Central Eastern Desert of Egypt. *Precambrian Res.* **1981**, *16*, 195–230. [CrossRef]
92. Stern, R.J.; Gottfried, D. Petrogenesis of a Late Precambrian (575–600 Ma) Bimodal Suite in Northeast Africa. *Contrib. Mineral. Petrol.* **1986**, *92*, 492–501. [CrossRef]
93. Hawkesworth, C.J.; Gallagher, K.; Hergt, J.M.; McDermott, F. Mantle and Slab Contributions in ARC Magmas. *Annu. Rev. Earth Planet. Sci.* **1993**, *21*, 175–204. [CrossRef]
94. Eby, G.N. Chemical Subdivision of the A-Type Granitoids: Petrogenetic and Tectonic Implications. *Geology* **1992**, *20*, 641. [CrossRef]
95. Eyal, M.; Litvinovsky, B.; Jahn, B.M.; Zanvilevich, A.; Katzir, Y. Origin and Evolution of Post-Collisional Magmatism: Coeval Neoproterozoic Calc-Alkaline and Alkaline Suites of the Sinai Peninsula. *Chem. Geol.* **2010**, *269*, 153–179. [CrossRef]
96. Davidson, J.P.; Ferguson, K.M.; Colucci, M.T.; Dungan, M.A. The Origin and Evolution of Magmas from the San Pedro-Pellado Volcanic Complex, S. Chile: Multicomponent Sources and Open System Evolution. *Contrib. Mineral. Petrol.* **1988**, *100*, 429–445. [CrossRef]
97. *ASTM C615/C615M*; Standard Specification for Granite Dimension Stone. American society for testing and materials: West Conshohocken, PA, USA, 2011.
98. Török, A.; Török, Á. The Effect of Temperature on the Strength of Two Different Granites. *Cent. Eur. Geol.* **2015**, *58*, 356–369. [CrossRef]
99. Siegesmund, S.; Dürrast, H. Physical and Mechanical Properties of Rocks. In *Stone in Architecture*; Siegesmund, S., Snethlage, R., Eds.; Springer: Berlin/Heidelberg, Germany, 2011; pp. 97–225. ISBN 978-3-642-14474-5.
100. Jain, N. Effect of Nonpozzolanic and Pozzolanic Mineral Admixtures on the Hydration Behavior of Ordinary Portland Cement. *Constr. Build. Mater.* **2012**, *27*, 39–44. [CrossRef]